AFGL-TR-88-0166

AD-A210 110

A New Background Stratospheric Aerosol
Model for Use in Atmospheric Radiation
Models

John R. Hummel
Eric P. Shettle
David R. Longtin

OptiMetrics, Inc
50 Mall Road
Burlington, MA 01803

30 July 1988

Scientific Report No. 8

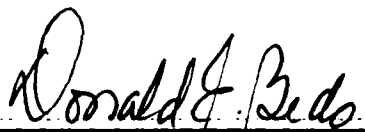APPROVED FOR PUBLIC RELEASE; DISTRIBUTION UNLIMITED

89   7   07   034

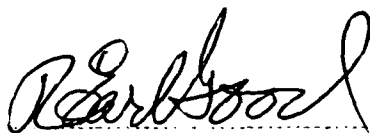"This technical report has been reviewed and is approved for publication"

ERIC P. SHETTLE
Contract Manager

DONALD E. BEDO
Branch Chief

FOR THE COMMANDER

R. EARL GOOD
Division Director

This report has been reviewed by the ESD Public Affairs Office (PA) and is releasable to the National Technical Information Service (NTIS)

Qualified requestors may obtain additional copies from the Defense Technical Information Center. All others should apply to the National Technical Information Service.

If your address has changed, or if you wish to be removed from the mailing list, or if the addressee is no longer employed by your organization, please notify AFGL/DAA, Hanscom AFB, MA 01731. This will assist us in maintaining a current mailing list.

Do not return copies of this report unless contractual obligations or notices on a specific document require that it be returned.

REPORT DOCUMENTATION PAGE

1a. REPORT SECURITY CLASSIFICATION	1b. RESTRICTIVE MARKINGS
Unclassified	
2a. SECURITY CLASSIFICATION AUTHORITY	3. DISTRIBUTION/AVAILABILITY OF REPORT
2b. DECLASSIFICATION/DOWNGRADING SCHEDULE	Approved for public release; distribution unlimited
4. PERFORMING ORGANIZATION REPORT NUMBER(S)	5. MONITORING ORGANIZATION REPORT NUMBER(S)
OMI-298	AFGL-TR-88-0166

6a. NAME OF PERFORMING ORGANIZATION	6b. OFFICE SYMBOL (If applicable)	7a. NAME OF MONITORING ORGANIZATION
OptiMetrics, Inc.		Air Force Geophysics Laboratory

6c. ADDRESS (City, State, and ZIP Code)	7b. ADDRESS (City, State, and ZIP Code)
50 Mall Road Burlington, MA 01803	Hanscom AFB, MA 01731-5000

8a. NAME OF FUNDING/SPONSORING ORGANIZATION	8b. OFFICE SYMBOL (If applicable)	9. PROCUREMENT INSTRUMENT IDENTIFICATION NUMBER
Air Force Geophysics Lab		F19628-85-C-0178

8c. ADDRESS (City, State, and ZIP Code)	10. SOURCE OF FUNDING NUMBERS			
	PROGRAM ELEMENT NO.	PROJECT NO.	TASK NO.	WORK UNIT ACCESSION NO.
Hanscom AFB, MA 01731-5000	6210F	7670	15	A1 16*

11. TITLE (Include Security Classification)

A New Background Stratospheric Aerosol Model For Use in Atmospheric Radiation Models

12. PERSONAL AUTHOR(S)
John R. Hummel, Eric P. Shettle**, and David R. Longtin

13a. TYPE OF REPORT	13b. TIME COVERED	14. DATE OF REPORT (Year, Month, Day)	15. PAGE COUNT
Scientific #8	FROM ___ TO ___	30 July, 1988	68

16. SUPPLEMENTARY NOTATION
*This work was partially accomplished with support from Inhouse Work Unit #7670 15 16   **Atmospheric Optics Branch, AFGL, Hanscom AFB, MA 01731-5000

17.	COSATI CODES		18. SUBJECT TERMS (Continue on reverse if necessary and identify by block number)
FIELD	GROUP	SUB-GROUP	Stratospheric Aerosols, Standard Radiation Atmosphere, LOWTRAN7, Atmospheric Radiation, Atmospheric Extinction

19. ABSTRACT (Continue on reverse if necessary and identify by block number)

The current AFGL background stratospheric aerosol model is based on laboratory measurements of indices of refraction for a solution of H_2SO_4 taken at 300 K and a size distribution based on a modified gamma distribution. Stratospheric temperatures are considerably colder than this. Also, recent satellite measurements indicate that a log normal size distribution is more representative of stratospheric aerosols. Therefore, a new background stratospheric aerosol model is presented based on temperature dependent indices of refraction and a log normal size distribution that is consistent with the literature.

A set of indices of refraction have been calculated using Lorentz-Lorenz corrections and interpolated values of the available laboratory measurements of the index of refraction of a mixture of 75% H_2SO_4 in water. Indices of refraction at 215 K have been taken as representative   (over)

20. DISTRIBUTION/AVAILABILITY OF ABSTRACT	21. ABSTRACT SECURITY CLASSIFICATION
☒ UNCLASSIFIED/UNLIMITED ☐ SAME AS RPT ☐ DTIC USERS	Unclassified
22a. NAME OF RESPONSIBLE INDIVIDUAL	22b. TELEPHONE (Include Area Code)	22c. OFFICE SYMBOL
Eric Shettle		AFGL/OPA

DD FORM 1473, 84 MAR 83 APR edition may be used until exhausted. SECURITY CLASSIFICATION OF THIS PAGE
All other editions are obsolete.

Unclassified

19. Abstract (continued)

of an averaged, midlatitude stratosphere. The log normal size distribution, based on recommendations from an experts meeting on aerosols and climatic effects held by the World Climate Programme.

The proposed formulation is compared against that of Shettle and Fenn[1]. The proposed extinction coefficients are essentially unchanged for wavelengths up to about 5 μm. Above 5 μm, the proposed values are smaller than that in LOWTRAN 6. The differences are due almost entirely to changes in the absorption coefficient as a result of the smaller imaginary components of the index of refraction. Also, the results are insensitive to changes in size distribution.

Contents

Contents

Illustrations

1. INTRODUCTION

Aerosols commonly found at stratospheric altitudes, 10 - 30 km, are a result of photochemical formation involving sulfur compounds. These background aerosols are generally uniform over the globe. The concentrations of these stratospheric aerosols can be increased dramatically following massive volcanic eruptions. Additional sulfur based aerosols can be photochemically created from the sulfur gases in an eruption cloud. Volcanic ash and debris can also be injected into these altitudes.

The Air Force Geophysics Laboratory (AFGL) has developed three stratospheric aerosol models[1] for use in the transmittance/radiance models LOWTRAN[2] and FASCODE[3]. The three models are for background stratospheric conditions, fresh volcanic aerosols, and aged volcanic aerosols. These models have also been adapted for use in the Standard Radiation Atmosphere (SRA)[4] models.

1. Shettle, E. P. and R. W. Fenn (1976) "Models of the Atmospheric Aerosols and Their Optical Properties," in AGARD Conference Proceedings No. 183, Optical Propagation in the Atmosphere. Presented at the Electromagnetic Wave Propagation Panel Symposium, Lyngby, Denmark, 27-31 October 1975, AGARD-CP-183, ADA028-615.

2. Kneizys, F. X., Shettle, E. P., Gallery, W. O., Chetwynd, J. H., Abreu, L. W., Selby, J. E. A., Clough, S. A., and Fenn, R. W. (1983) Atmospheric transmittance/radiance: Computer code LOWTRAN 6, AFGL-TR-83-0187, AD 137796.

3. Clough, S. A., Kneizys, F. X., Shettle, E. P., and Anderson, G. P. (1986) Atmospheric radiance and transmittance: FASCOD2, Proceedings of the Sixth Conference on Atmospheric Radiation, Williamsburg, Virginia, American Meteorological Society, Boston, Massachusetts, 141-144.

4. WCP (1986) A preliminary cloudless standard atmosphere for radiation computation, WCP-112, WMO/TD-No 24,

The background stratospheric aerosol consists of a 75 % solution of sulfuric acid in water. The wavelength dependent index of refraction for the solution is based on laboratory measurements at 300 K[5,6,7]. The indices of refraction for the volcanic ash are based on measurements of Volz[8]. The size distributions for all three stratospheric aerosols are given by modified gamma distributions.

Stratospheric temperatures are well below 300 K. Values of the index of refraction for H_2SO_4 are now available at 250 K[9] and can be used to calculate temperature dependent indices of refraction for H_2SO_4 for temperatures appropriate for stratospheric conditions. Also, recent measurements of the size distribution of stratospheric aerosols indicate that a log normal distribution may be more appropriate for stratospheric aerosols than a modified gamma distribution[10].

World Climate Research Programme, International Association of Meteorology and Atmospheric Physics/Radiation Commission.

5. Remsberg, E. E. (1971) Radiative properties of several probable constituents of Atmospheric Aerosols, PhD. Thesis, Department of Meteorology, University of Wisconsin, Madison.

6. Remsberg, E. E. (1973) Stratospheric aerosol properties and their effects on infrared radiation, J. Geophys. Res., 78:1401-1407.

7. Palmer, K. F. and D. Williams (1975) Optical constants of sulfuric acid; Application to the clouds of Venus?, Applied Optics, 14:208-219.

8. Volz, F. E. (1973) Infrared optical constants of ammonium sulfate, Sahara dust, volcanic pumice, and flyash, Appl. Opt., 12:564-568.

9. Pinkley, L. W. and Williams, D. (1976) The infrared optical constants of sulfuric acid at 250 K, J. Opt. Soc. Am., 66:122-124.

10. WCP (1983) Report of the Experts Meeting on Aerosols and Their Climatic Effects , Eds. Deepak, A. and Gerber, H. E., World Climate Programme, WCP 55, World Meteorological Organization, p 30.

1.1 Organization of Report

This report describes the development of a new background stratospheric aerosol model in which temperature dependent indices of refraction for H_2SO_4 have been used with a log normal size distribution. Chapter 2 is a summary of the literature that provides the justification for the development of a new model. Chapter 3 describes the methodology used to formulate the new model. Chapter 4 presents results from the new formulation and compares them against the formulation currently used. Finally, Chapter 5 presents the conclusions and recommendations for future work.

2. A REVIEW OF STUDIES OF STRATOSPHERIC AEROSOLS

Two recent major volcanic eruptions have provided researchers with the opportunity to study stratospheric and volcanic aerosols in depth. The eruptions were Mt. St. Helens in 1980 and El Chichon in 1982. In both cases, the eruptions were intensely studied by ground and aircraft based lidars, balloons, aircraft and satellites.

2.1 Lidar Studies

Lidar provides a tool to study particulate matter in the stratosphere. Lidars at various locations around the world have permitted researchers to study the distribution of volcanic materials injected into the stratosphere since the 1970's. The altitude resolution that can potentially be obtained from lidars allows researchers to study both the temporal and spatial details of volcanic eruption clouds. The worldwide network of lidars (e.g.[11,12,13,14,15,16]) pro-

11. Reiter, R., Jager, H., Carmuth, W., and Funk, W. (1979) The stratospheric aerosol layer observed by lidar since October 1976. A contribution to the problem of hemispheric climate, Arch. Met. Geoph. Biokl., Ser. B, 27:121-149.
12. D'Altorio, A., Viconti, G., and Fiocco, G. (1981) Lidar detection of volcanic aerosols in the atmosphere following the Mount St. Helen eruption, Geophys. Res. Let., 8:63-65.
13. Clemesha, B. R. and Simmonich, D. M. (1978) Stratospheric dust measurements, 1970-1977, J. Geophys. Res., 83:2403-2408.
14. Iwasaka, Y., Hayashida, S., and Ono, A. (1983) Increasing backscattered light from the stratospheric aerosol layer radar after Mt. El Chichon eruption, laser radar Measurement at Nagoya (35°N, 137°E), Geophys. Res. Let., 6:440-442.
15. Hirono, M., Fujiwara, M., Shibata, T., and Kugumiya, N. (1981) Lidar observations of Mt. St. Helens in May 1980, Geophys. Res. Let., 9:1019-1022.

vided extensive coverage of the eruption clouds from the Mount St. Helens and El Chichon eruptions. These lidars have also detected the presense of so-called "mystery clouds", clouds that cannot be traced to the eruption of known volcanoes.

The lidars used for probing the upper troposphere and stratosphere use the lidar backscattering ratio to identify layers of non-molecular scattering. The lidar back-scattering ratio as a function of altitude, $B(z)$, is given as

$$B(z) = 1 + f_A(z)/f_M(z) \qquad (1)$$

where $f_A(z)$ is the aerosol backscattering function and $f_M(z)$ is the molecular backscattering function. A requirement for the use of (1) is the assumption that at some altitude the returned lidar signal is only from molecular scatterers. This altitude, often called the matching altitude, is used to determine the atmospheric density profile required to give $f_M(z)$. Once this is known, any return greater than that produced by a pure molecular atmosphere is assumed to be from particulates. The matching altitude is generally taken to fall in the 30 km range, although Clemesha and Simonich[13] feel that the matching altitude should be taken at higher altitudes.

16. McCormick, M. P., Swissler, T. J. (1983) Stratospheric aerosol mass and latitudinal distribution of the El Chicon eruption cloud for October 1982, Geophys. Res. Let., 9:877-880.

Table 1 summarizes results[12,13,14,15,17,18,19,20,21] of lidar studies made under background and volcanic conditions. The studies indicate that a backscatter ratio of between 1.1 and 1.4 is representative of background stratospheric conditions. The backscatter ratio following an eruption is highly variable and depends on the force of the eruption, as measured by the amount of material injected and the height of the eruption cloud, as well as the sulfur content of the eruption cloud.

The lidar studies have detailed the layering of material following volcanic eruptions. The layers are highly dynamic and can change somewhat quickly as a result of variations in the stratospheric circulation and as particles settle out.

17. Clemesha, B. R. and Simmonich, D. M. (1983) Lidar observations of the El Chicon dust cloud at 23°S, Geophys. Res. Let., 10:321-324.
18. Hirono, M., Fujiwara, M., and Shibata, T. (1981) Lidar observation of sudden increases of aerosols in the stratosphere caused by volcanic injections. I. Soufriere 1979 event, J. Atmos. Terr. Phy, 43:1127-1131.
19. Hirono, M., Fujiwara, M., and Shibata, T. (1982) Lidar observation of sudden increases of aerosols in the stratosphere caused by volcanic injections. II. Sierra Negra event, J. Atmos. Terr. Phy, 44:811-818.
20. Hirono, M. and Shibata, T. (1983) Enormous increase of stratospheric aerosols over Fukuoro due to volcanic eruption of El Chicon in 1982, Geophys. Res. Let., 10: 152-154.
21. D'Altorio, A. and Visconti, G. (1983) Lidar observations of dust layers' transience in the stratosphere following the El Chichon volcanic eruption, Geophys. Res. Let., 10:27-30.

Table 1. Summary of Lidar Studies of Background and Volcanic Aerosol Conditions in the Stratosphere

LOCATION	TIME PERIOD	WAVELENGTH (μm)	ALTITUDE REGION (km)	AVERAGE BACKSCATTER RATIO
Brazil[13,17] (23°S, 46°W)	July-August 1970	0.589	20	1.4
	1973	0.589	20	1 06 - 1.12
	August 1975	0.589	20	1.28
	April 1976	0.589	20	1.15
	1982	0.589	15 - 20	> 5.0 (Peak)
Japan (33°N, 130°E) (Ref 14,15, 18,19,20)	May 1978-Apr 1979	0.694	16	1.052 ± 0.02
	May-June 1979	0.694	16	$1.12 - 1.4\overline{2}$
	May 1978-Apr 1979	0.694	20	1.116 ± 0.05
	Nov 1979	0.532	21	1.05
	Nov 1979	1.064	21	1.46 ± 0.19
	Dec 1979	0.532	21	1.2 (Peak)
	Dec 1979	1.064	21	2.0 (Peak)
	Apr 1982	0.532	24.5	400 (Peak)
Japan[20] (35°N, 137°E)	Apr-July 1982	0.694	24 - 26	44 (Peak)
Italy[12] (42°N, 23°E)	Sept-Dec 1979	0.589	14 - 20	< 1.2
	June-July 1980	0.589	14 - 20	2.0
Italy[21] (42°N, 13°E)	Mar-Apr 1982	0.589	15 - 25	1.5 (Peak)

2.2 Balloon Measurements

Hofmann and Rosen have made extensive measurements of background stratospheric[22] and volcanic aerosols[23,24,25] using balloon-borne instruments that can reach altitudes up to about 35 km. Their typical balloon package carries optical particle counters to measure condensation nuclei for particles with radii $r \geq 0.01$ µm and a dustsonde for particles with $r \geq 0.15$ and $r \geq 0.25$ µm. A more recent version[24] also carries a large particle counter for $r > 0.25$, 0.95, 1.2 and 1.8 µm.

The particle size measurements provide integral values of the particle concentrations with sizes greater than or equal to the respective cut-off radii. By taking ratios of these concentrations, a set of size ratios can be obtained that can be related to size distribution.

The balloon packages have also been equipped with an intake heater that heats the air samples to around 150° C. This allows one to distinguish from volatile and nonvolatile aerosols. This technique has identified the volatile

22. Rosen, J. M., Hofmann, D. J., and Laby, J., (1975) Stratospheric aerosol measurements, II, Worldwide distribution, J. Atmos. Sci., 32:1457-1462.
23. Hofmann, D. J., and Rosen, J. M., (1982) Balloon-borne observations of stratospheric aerosol and condensation nuclei during the year following the Mt. St. Helens Eruption, J. Geophys. Res., 87:11039-11061.
24. Hofmann, D. J., and Rosen, J. M., (1983) Stratospheric sulfuric acid fraction and mass estimate for the 1982 volcanic eruption at El Chichon, Geophys. Res. Let, 10:313-316.
25. Hofmann, D. J., and Rosen, J. M., (1984) On the temporal variation of stratospheric aerosol size and mass during the first 18 months following the 1982 eruption of El Chichon, J. Geophys. Res., 89:4883-4890.

aerosols as having an average mixture of 75 % H_2SO_4 and 25 % H_2O.

The balloon measurements of background conditions yielded average peak aerosol concentrations that would correspond to back scattering ratios of about 1.09 - 1.17 at 0.6943 μm[26]. These results agree well with the lidar results summarized in Table 1.

Hofmann and Rosen conducted thirty six balloon flights from Laramie, Wyoming (41° N) to study the Mt. St. Helens eruption cloud during the year following the eruption[23]. The Mt. St. Helens eruption cloud was observed as four different layers at different altitudes over the 12 - 24 km region. The cloud was first observed at about 12 - 15 km in the vicinity of the jet stream. After about a week, a layer appeared in the 15 - 18 km range over Laramie. This layer became the main layer from the eruption. Material was also injected into the 18 - 24 km range where the summer stratospheric winds shift from westerlies to easterlies. The third layer was at 18 - 20 km where the winds were shifting and the fourth at 20 - 24 km where the winds were blowing from the east.

Hofmann and Rosen also studied the El Chichon cloud for eighteen months following its eruption[24,25]. Those flights were from Laramie and from locations in southern Texas (27° N - 29 °N).

---
26. Pinnick, R. G., Rosen, J. M., and Hofmann, D. J., (1976) Stratospheric aerosol measurements, III, Optical model measurements, J. Atmos. Sci., 33:304-314.

The flights discovered two major layers of aerosols separated by a very clean region. The first was around the tropopause and extended to about 21 km. The second layer was centered around 25 km and was generally about 5 km thick. The two layers may have resulted from two separate eruptions. The lower layer may have resulted from the initial 28 March 1982 eruption while the higher one may have come from the more violent 4 April 1982 eruption.

The upper layer was dominated by larger particles consisting of a mixture of about 80 % H_2SO_4 and 20 % H_2O while the lower layer consisted of an aerosol with a concentration of 60 - 65 % sulfuric acid. The difference in acid concentration was due to the warmer temperatures and lower water vapor abundances in the upper layer.

Table 2 shows the peak aerosol concentrations measured above 20 km from the two locations as a function of time following the eruption. The data displayed only cover three of the size ranges measured. Data from a flight on February 5, 1982 are given as representative of pre-eruption values. The differences between the two locations result from the Texas flights penetrating denser regions of the eruption cloud.

The size distribution determined from balloon measurements taken 45 days after the eruption was bimodal with mode radii of 0.02 and 0.7 μm. After about June 1982, the production of condensation nuclei (e.g., the curve of $r \geq 0.01$ μm)

had essentially ceased and fallen back to pre-eruption values.

Table 2. Peak Aerosol Concentrations Above 20 km for Three Size Ranges As a Function of Time After the Eruption of El Chichon as Measured from Laramie, Wyoming and Southern Texas[26]. The data from 2/5/82 are given as representative of pre-eruption values

DAYS AFTER ERUPTION	PEAK AEROSOL CONCENTRATIONS					
	$r \geq 0.01\,\mu m$ $(\# \; cm^{-3})$		$r \geq 0.15\,\mu m$ $(\# \; cm^{-3})$		$r \geq 0.25\,\mu m$ $(\# \; cm^{-3})$	
	Wyo	Texas	Wyo	Texas	Wyo	Texas
(2/5/82)	8		0.5		0.1	
2	25		0.8		0.1	
10	50		0.8		0.1	
20	48		0.7		0.1	
40	45		0.65		0.13	
45		700		22		16
60	38	400	0.6	20	0.16	15
73	400		4.0		1.1	
80	200	160	4.2	16	2.0	13
95	45		8.0		6.0	
100	38	65	5.0	15	3.0	11
110	23		2.0		1.2	
120	24	30	4.0	12	2.8	10
125	24		5.2		4.0	
140	15	12	4.0	11	2.8	0.9
152	10		3.5		2.0	
160	13	13	5.0	11.5	4.0	0.85
178	10		1.8		0.8	
180	11	13.5	2.3	11	1.0	0.8
190	13		10.0		2.0	
200	12	14	7.0	10	2.5	0.7
215	11		4.0		3.0	
220	10		5.0		3.2	
240	10		7.1		5.2	

2.3 Aircraft Measurements

Extensive aircraft measurements of stratospheric aerosols were made of the Mt. St. Helens and El Chichon

eruptions. Flight paths were often chosen to overlap other measurements such as the balloon measurements of Hofmann and Rosen.

2.3.1 Size Distribution Measurements

Oberbeck et al.[27] collected particles from the Mt. St. Helens eruption cloud for a year using wire impactors flown upon the NASA U-2. The aircraft sampled the stratospheric aerosols at an altitude of 18.3 km, the height where the main aerosol layer eventually formed.

Table 3 shows the sampled aerosol particle concentrations for two size ranges, $r < 0.15$ µm and $r > 0.15$ µm, for the year following the eruption. In the six months after the eruption, the total volume of aerosols with radii greater than 0.03 µm increased. The concentration of particles with radii less than 0.15 µm decreased while the concentration of particles with radii greater than 0.15 µm increased. This is consistent with the dispersal of an initially high concentration of small particles and the growth of aerosols by condensation. The aerosol levels returned to normal in about a year.

The El Chichon eruption was well studied by aircraft. One series of measurements involved measuring stratospheric size distributions with "Knollenberg" counters[28]. The mea-

27. Oberbeck, V. R., Farlow. N. H., Fong, W., Snetsinger, K. G., Ferry, G. V. Ferry and Hayes, D. M., (1982) Mount St. Helens aerosol evolution, Geophys. Res, Let., 9:1089-1092.
28. Knollenberg, R. G., and Huffmann, D., (1983) Measurements of the aerosol size distributions in the El Chichon cloud, Geophys. Res. Let., 10:1025-1028.

surements made prior to the eruption revealed relatively featureless size distributions. The data over the range 0.1 to 1.0 μm revealed particles that were largely H_2SO_4. Their number density varied with altitude from about 20 cm-^{3} at 17 km to about 1 cm^{-3} at 20 km.

Table 3. Aerosol Concentrations From the Mt. St. Helens Eruption Cloud at 18.3 km in two Size Ranges as Measured by Wire Impactor[27]

DATE	MONTHS AFTER ERUPTION	$r > 0.15$ μm (cm^{-3})	$r < 0.15$ μm (cm^{-3})
5/20/80	0	2.0	11.0
6/25/80	1	1.8	22.5
7/16/80	2	2.5	18.0
10/29/80	5	3.5	14.0
12/2/80	6.5	4.0	15.0
12/17/80	7	2.5	6.0
4/10/81	12	1.5	3.0

Flights following the eruption suggested two dominant size modes. The first mode consisted of small particles (0.1 - 0.8 μm) that were primarily H_2SO_4 and large particles (0.8 - 30 μm) that were primarily volcanic ash. Later flights indicated that particles up to 2.0 μm were largely H_2SO_4 although some of the particles may have been coated with sulfuric acid.

Oberbeck et al.[29] also studied the El Chichon eruption cloud with the Ames Wire Impactor. Table 4 summarizes the total aerosol concentrations as measured at different altitudes. The size distribution measured prior to the eruption could be fitted with a log normal distribution with a total concentration of between 3.4 and 4.3 cm^{-3}, a mode radius of 0.08 µm and a standard deviation of about 1.68. After the eruption, the distribution was best represented with two log normal size distributions, an enhanced background of sulfuric acid particles with a larger mode radius and a sedimentation mode consisting of large silicates.

Table 4. Total Aerosol Concentrations From the El Chichon Eruption Cloud at Various Altitudes as Measured by the Ames Wire Impactor[29]

DATE	MONTHS AFTER ERUPTION	ALTITUDE (km)	N (cm^{-3})
10/16/81	–	18.3	6.3
5/5/82	1	20.7	3.9
7/23/82	3.5	20.7	7.8
9/23/82	5.5	19.8	13.68
11/4/82	7	20.7	6.2
11/5/82	7	20.7	5.4
12/13/82	8	20.7	7.9

29. Oberbeck, V. R., Danielsen, E. F., Snetsinger, K. G., Ferry, G. V. Fong, W., Hayes, D. M., (1983) Effect of the eruption of El Chichon on stratospheric aerosol size and composition, Geophys. Res. Let., 10:1021-1024.

Wilson et al.[30] summarized many of the NASA U-2 measurements made at 20 km of sub-2.5 μm diameter aerosols following the El Chichon eruption. Their results indicated that the background aerosols were dominated by particles with radii smaller than 0.05 or 0.03 μm. Measurements in April and May 1982 indicated significant increases in the sub 0.1 μm aerosol concentration that can only be explained by gas-phase reactions leading to the formation of secondary (non-eruption) aerosols. Measurements in the same size range made in late 1982 showed considerable depletion suggesting coagulation of small particles to form larger ones.

2.3.2 Transmission Measurements

Witteborn et al.[31] obtained infrared transmission spectra for the atmosphere above 11 km for latitudes between 2° S and 50° N. The measurements were made in December 1982 when the stratospheric aerosols were still considerably enhanced by the El Chichon eruption. The absorption was obtained by ratioing the transmission at 8.5 μm, where the H_2SO_4 absorption is strongest, to that at 12 μm, where the atmospheric transmission is nearly unity. The average absorption per unit air mass was evaluated at 0.019, of which 0.010 was attributable to the presence of H_2SO_4 aerosols.

30. Wilson, J. C., Blackshear, E. D., and Hyun, J. H., (1983) Changes in the sub-2.5 micron diameter aerosol observed at 20 km altitude after the eruption of El Chichon, Geophys. Res. Let., 10:1029-1032.
31. Witteborn, F. C., O'Brien, K., Crean, H. W., Pollack, J. B., and Bilski, K. H., (1983) Spectroscopic measurements of the 8- to 13-micrometer transmission of the upper atmosphere following the El Chichon eruptions, Geophys. Res. Let., 10:1009-1012.

They also reported that the ratio of optical depth at 8.5 μm to that at 0.5 μm, obtained by Dutton and DeLuisi[32] was about 0.14 at 20° N.

2.3.3 Composition Measurements

Woods and Chuan[33] sampled the El Chichon volcanic cloud using a quartz crystal microbalance (QCM) cascade impactor flown on the NASA U-2. The QCM collected and classified particles into 10 size intervals from less than 0.05 μm to greated than 25 μm diameter. The collected aerosols were then analyzed for composition.

The compositional analysis indicated that the submicron particles were largely sulfuric acid droplets. This is contrasted with Mt. Agung in which the primary component was volcanic ash. Their measurements of the sulfuric acid aerosols indicated that they occurred in a relatively narrow size range with diameters from about 0.08 to 0.45 μm. Particles above this range were primarily lithic and magmatic materials from the volcano. Halite particles were also found and were believed to be from a salt dome that was located beneath El Chichon.

Patterson and coworkers have measured the optical properties of volcanic ash in visble wavelength for ash from Mt.

32. Dutton, E., and DeLuisi, J., (1983) Extinction of solar radiation by the El Chichon dust cloud, Geophys. Res. Let., 10:1013-1016.
33. Woods, D. C., and Chuan, R. L., (1983) Size-specific compositions of aerosols in the El Chichon volcanic cloud, Geophys. Res. Let., 10:1041-1044.

St. Helens[34] and El Chichon[35]. Their studies indicate that the imaginary component of the refractive index of the ash varies from volcano to volcano. The Mt. St. Helens ash had an imaginary component that decreased from about 0.01 at 0.3 µm to about 0.0015 at 0.7 µm. The corresponding values for the El Chichon ash were nearly constant at 0.001 over the same wavelength range.

2.4 Size Distribution Studies Using Satellite Data

A new series of satellites have been launched that offer new details of the background and perturbed stratosphere. These satellites have include the Stratospheric Aerosol and Gas Experiment (SAGE I & II) and the Stratospheric Aerosol Measurement (SAM I & II) sensors. Although not explicitly designed to study stratospheric aerosols, the Solar Mesosphere Explorer spacecraft was also able to study the El Chichon eruption.

The SAM II sensor has a single pass band centered at 1.0 µm. Gaseous absorption is negligible at this wavelength, so the measured extinction is due to molecular and aerosol scattering. The molecular scattering is filtered out during data processing leaving only the aerosol component. Russell et al.[36] performed a comparison of SAM

34. Patterson, E. M. (1981) Measurements of the imaginary part of the refractive index between 300 and 700 nanometers for Mount St. Helens ash, Science, 211:836-838.
35. Patterson, E. M., Pollard, C. O., and Galindo, I., (1983) Optical properties of the ash from El Chichon, Geophys. Res. Let., 10:317-320.
36. Russell, P. B., McCormick, M. P.,Swissler, T. J. Chu, W.P., Livingston, J. M., Fuller, W. H , Rosen, J. M., Hofmann, D. J., McMaster, L. R., Woods, D. C. and

II extinction profiles against profiles inferred from balloon-borne dustsondes and an airborne lidar. Their results indicated that the different sensors agreed within their respective measurement and conversion uncertainties.

The SAGE I sensor system consists of four wavelengths with two of them, centered at 0.45 and 1.0 μm, designed for aerosol studies. The two channels, used together, provide extinction profiles and size distribution data.

Lenoble et al.[37] used 93 SAGE I profiles of the extinction coefficients at 1.0 and 0.45 μm from July 1980 to study the variation of the aerosol size distributions in the Mount St. Helens aerosol layer. The measurements were made between 50 and 70° N. Further measurements from May to November 1980 showed a low layer cloud of primarily large particles and a higher altitude cloud of small particles. The size distributions within the clouds were assumed to be log normal and the clouds were assumed to be made up of 75 % H_2SO_4 droplets in solution with H_2O. Using Mie theory, the mode radii of the layers were inverted. The low layer cloud was found to have an average logarithmic mode radius of 0.20 μm while the high altitude cloud had a logarithmic mode radius of 0.06 μm. Logarithmic mode radii corresponding to

Pepin, T. J. (1981) Satellite and correlative measurements of the stratospheric aerosol. II: Comparison of measurements made by SAM II, dust-sondes and an airborne Lidar, J. Atmos. Sci., 38: 1295-1312.

37. Lenoble. J., Pruvost, P. and Brogniez, C. (1984) SAGE satellite observations of stratospheric aerosols from Mount St. Helens eruption: A two-wavelength analysis, J. Geophys. Res., 89:11666-11676.

individual orbits were given for approximately 0.2 degree intervals from $50°$ to $65°$ N latitudes.

Latitudinally averaged results were given as a function of time that demonstrate the temporal variation of the size distributions as the larger particles settle out. Those results are given in Table 5.

Table 5. Latitudinally Averaged Mode Radii, in μm, for a Log Normal Size Distribution as a Function of Time Between $55°$ N and $65°$ N Latitudes Following the Mount St. Helens Eruption[37]. These values assume a standard deviation of 1.604

LAYER (km)	June 23 to July 20		July 20 to Aug 28		Aug 28 to Sept 28		Sept 28 to Oct 31	
	$55°$	$65°$	$55°$	$65°$	$55°$	$65°$	$55°$	$65°$
18-20	---	0.151	0.142	0.146	0.142	0.137	0.142	0.142
22-23	---	0.084	0.090	0.073	0.100	0.100	0.106	0.103

Brogniez and Lenoble[38] have also used SAGE I profiles to study background stratospheric aerosol conditions. From the tropopause to about 10 km above the tropopause, the background extinction coefficient at 1.0 μm is nearly constant at all latitudes and seasons at 1.20×10^{-4} km. Above this altitude, the background extinction coefficient profile can be fitted with an exponential with an average scale height of 3.2 km. The altitude where the profiles change

---

38. Brogniez, C., and Lenoble, J., (1987) Modeling of the stratospheric background aerosols from zonally averaged SAGE profiles, J. Geophys. Res., 92:3051-3060.

from constant to an exponential decrease is a function of latitude and season. The transition altitude is highest for high latitude winters and lowest for high latitude summers.

Their values can be compared to those in the (SRA) model[2]. The SRA model gives an extinction coefficient of 0.68×10^{-4} km^{-1} for 1.0 µm for the altitudes 12 - 20 km. Above 20 km, the decrease in extinction coefficient is linear.

3. METHODOLOGY

3.1 Calculating the Temperature Dependence of the Index of Refraction of H_2SO_4 Droplets

The temperature dependence of sulfuric acid droplets for wavelengths far from absorption features can be calculated using the Lorentz-Lorenz relationship. The Lorentz-Lorenz relationship relates the complex index of refraction, m, to the molecular polarizability per unit volume

$$\rho = \frac{3V}{4\pi} \frac{(m^2 - 1)}{(m^2 + 2)} \qquad (2)$$

where ρ is the density. The Lorentz-Lorenz equation is a form of the Clausius-Mossotti equation that established that $(\epsilon - 1)/(\epsilon + 2)$ should be proportional to the density of a substance, where ϵ is the dielectric constant. Eq. (2) is obtained by setting $\epsilon = m^2$. According to Jackson[39] and Mayer and Mayer[40], the proportionality to density holds for gases but is only an approximation for liquids. Pinkley and Williams[9] have observed experimentally that the Lorentz-Lorenz relationship appears to be valid away from absorption bands, but fails near strong bands for liquids.

Under the assumption that the relationship is valid for a solution of H_2SO_4 and water, the Lorentz-Lorenz relationship can be expressed as

39. Jackson, J. D. (1975) Classical Electrodynamics, John Wiley & Sons, 2 nd Edition, New York, p 155.
40. Mayer, J. E., and Mayer, M. G. (1940) Statistical Mechanics, John Wiley & Sons, New York, p 340.

$$\frac{(m^2 - 1)}{(m^2 + 2)} = A \rho(T) \tag{3}$$

where A is a constant and ρ (T) is the temperature dependent H_2SO_4 solution density. Letting m_1 be the index of refraction at a temperature T_1 and m_2 be the index of refraction at temperature T_2, then

$$\frac{(m_2^2 - 1)}{(m_1^2 + 2)} = \frac{\rho_2}{\rho_1} \frac{(m_1^2 - 1)}{(m_1^2 + 2)} \tag{4}$$

or, with a little algebra

$$m_2 = \left[\frac{1 + 2D}{1 - D}\right]^{1/2} \tag{5}$$

where D is given by

$$D = \frac{\rho_2}{\rho_1} \frac{(m_1^2 - 1)}{(m_1^2 + 2)} \tag{6}$$

The temperature dependent density data of a 75 % solution of H_2SO_4 and water[41] used in the calculations are shown in Figure 1.

For wavelength regions in the vicinity of absorption features, the Lorentz-Lorenz relationship is not valid. In those regions, a linear interpolation and extrapolation of the available data was performed. For the imaginary components, the interpolation was performed in terms of the logarithm of the value. For wavelengths above 3.0 μm, the

41. Roth, W. A. and Scheel,K., eds. (1923) Landolt-Born-stein Physikalisch-Chemische Tabellen, Verlag von Julius, Springer, Berlin, 397-398.
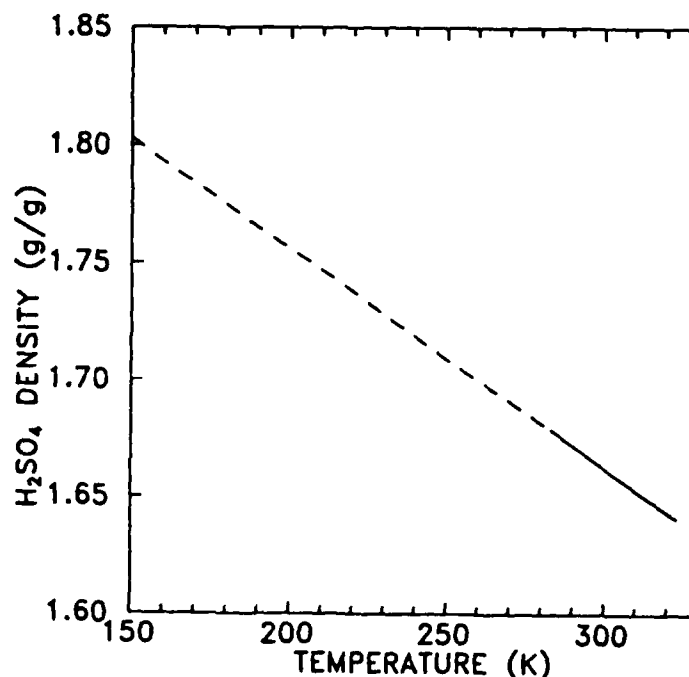
Figure 1. The Density of a Mixture of 75% H_2SO_4 and 25% H_2O as a Function of Temperature[41]. The dashed portion indicates the extrapolated values

interpolation procedure was performed using the data discussed below at 300 K and the data of Pinkley and Williams[9] at 250 K. The earlier values of Shettle and Fenn[1], based on an average of the data of Palmer and Williams[7] and Remsberg[5,6] were used for wavelengths up to 25 μm. Between 20 and 50 μm, the data of Jones[42] were used. Between 50 and 300 μm, an interpolation of qualitative results from the work of Rossow and Sagan[43] were used to

42. Jones, A. D. (1976) Optical constants of sulfuric acid in the far infrared, *J. Quant. Spectrosc. Radiat. Transfer*, 16:1017-1019.
43. Rossow, W. B., and Sagan, C., (1975) Microwave boundary conditions on the atmosphere and clouds of Venus, *J. Atmos. Sci.*, 32:1164-1176.

23

extend the values for both temperatures. Those results assumed that the imaginary part of the index of refraction reached a maximum at 150 cm^{-1} and decreased linearly with frequency to about 10 cm^{-1}. The real part was assumed to varying linearly with frequency between 40 and 1000 μm, reaching about 2.1 at 1000 μm.

3.2 Proposed Size Distribution

The log normal size distribution parameters suggested by the World Meteorological Organization's Experts Meeting[10] will be used. These parameters are consistent with those based on the review of various measurements discussed in Chapter 2. The distribution is given by

$$n(r) = \frac{d\ N(r)}{d\ \log\ r} = \frac{N_o}{\sqrt{2\pi}\ \log\ \sigma}\ \exp\ \left(-\frac{1}{2}\left[\frac{\log\ (r/R)}{\log\ \sigma}\right]^2\right) \quad (7)$$

The extinction coefficient values produced by (7) have been scaled to give $1.2 \times 10^{-4}\ km^{-1}$ at 1.0 μm, the average SAGE I value reported by Brogniez and Lenoble[38]. The resultant values are a total number density, N_o, of 9 cm^{-3}, a mode radius, R, of 0.06951 μm and a standard deviation, σ, of 1.86. Figure 2 compares the modified gamma function used by Shettle and Fenn[1] and the proposed log normal size distribution.
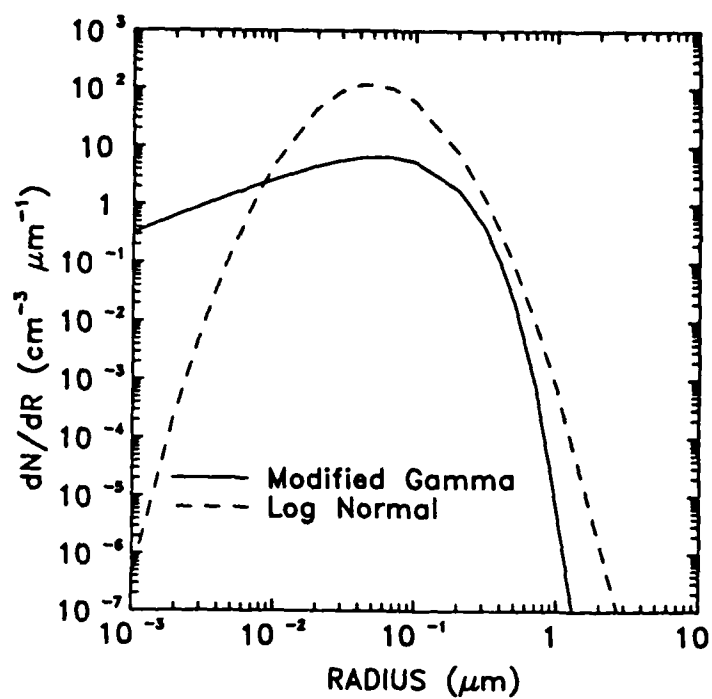
Figure 2. Comparison of the Modified Gamma Function Size
Distribution Used in Shettle and Fenn[1] and the Proposed Log
Normal Size Distribution

4. RESULTS

4.1 Indices of Refraction

Calculations for temperature dependent indices of refraction were performed for temperatures from 150 to 290 K. The calculations were done for 68 wavelengths between 0.2 and 300 μm. The Lorentz-Lorenz relationship was used for wavelengths below 3.0 μm with data obtained at 300 K used as reference[7]. For wavelengths above 3.0 μm, values were interpolated as described in Section 3.1. The values are listed in Table 6.

Figure 3 shows the temperature dependence of the real component of m at 0.55 μm. At this wavelength, the imaginary component is on the order of 10^{-8} and is nearly temperature independent. The inflection points seen near 160, 220 and 280 K are a result of truncating the refractive index values to three significant figures. Figures 4 (a) and (b) show, respectively, the real and imaginary components at 10 μm as a function of temperature.

Indices of refraction at 215 K will be taken as representative of stratospheric temperatures and used to determine the extinction coefficients for the proposed background stratospheric aerosol model. The indices of refraction at 215 K are listed in Table 6 and the real and imaginary parts shown, respectively, in Figures 5 (a) and (b) as a function of wavelength. The values at 300 K, at 250 K, and at 150K are also shown for comparison.
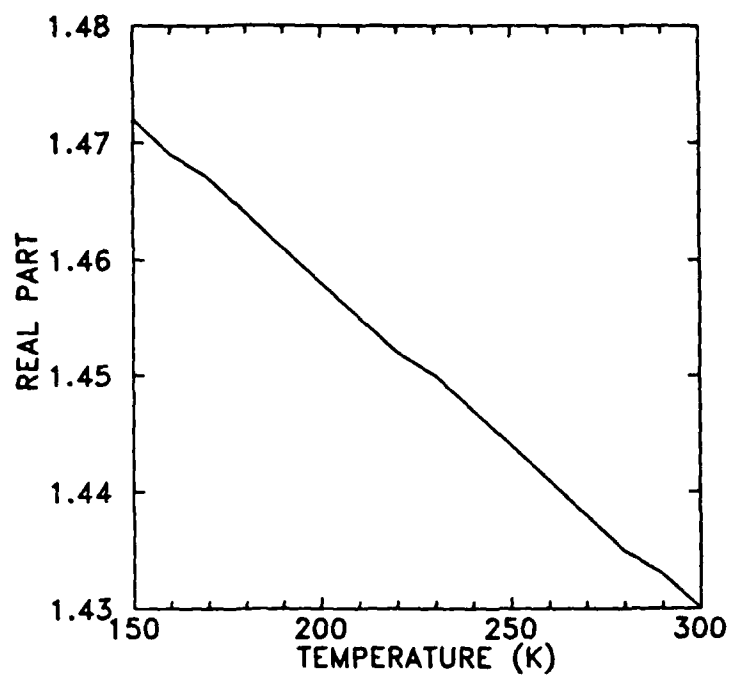
Figure 3. The Real Part of the Index of Refraction at
0.55 μm of a Mixture of 75% H_2SO_4 and 25% H_2O as a Function
of Temperature. The inflection points that appear near 160,
220, and 280 K are a result of truncating the refractive
index values to three significant figures
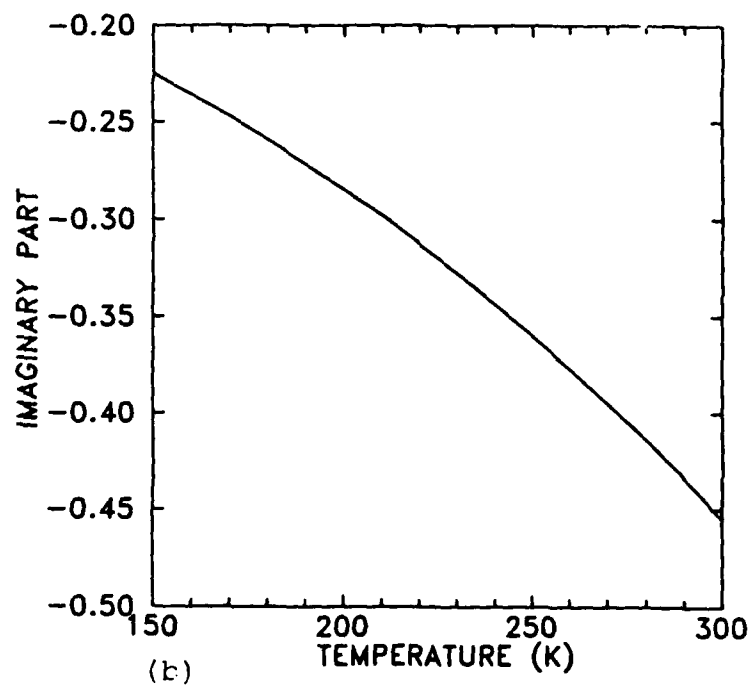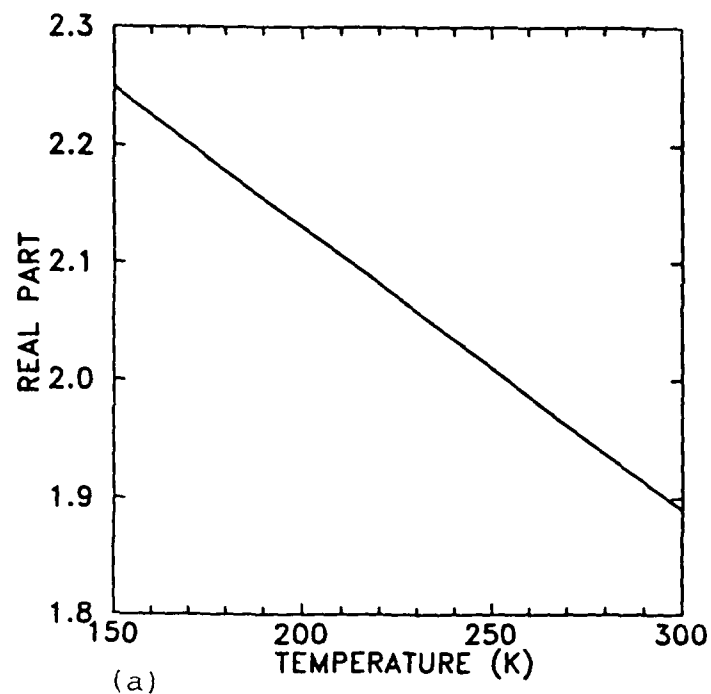
Figure 4. The (a) Real and (b) Imaginary Parts of the Index
of Refraction at 10 μm of a Mixture of 75% H_2SO_4 as a
Function of Temperature
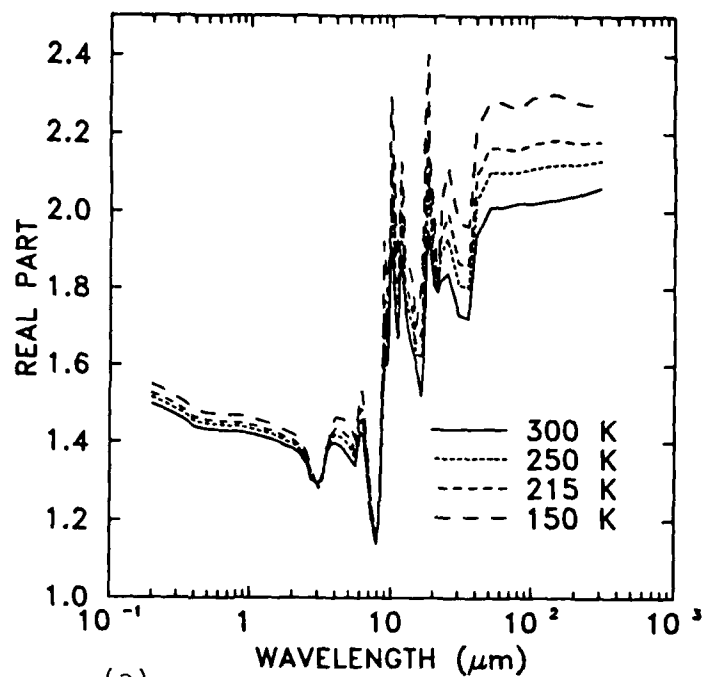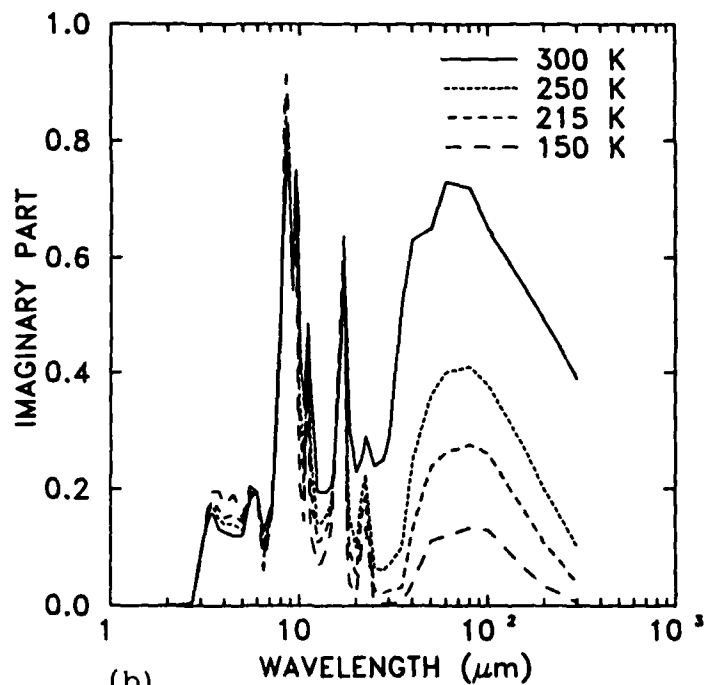
Figure 5. The (a) Real and (b) Imaginary Parts of the Index of Refraction for a 75% Sulfuric Acid Solution at 300, 250, 215 K and 150 K as a Function of Wavelength

Table 6. Real, n_r, and Imaginary, n_i, Indices of Refraction for a 75 % Solution of Sulfuric Acid Droplets at 215 K. The values in parentheses indicate the power of 10 by which n_i should be multiplied

LAMBDA (μm)	n_r	n_i	LAMBDA (μm)	n_r	n_i
0.2000	1.526	-1.07(-8)	8.5000	1.457	-0.840
0.2500	1.512	-1.07(-8)	8.7000	1.753	-0.817
0.3000	1.496	-1.07(-8)	9.0000	1.767	-0.604
0.3371	1.484	-1.07(-8)	9.2000	1.704	-0.557
0.4000	1.464	-1.07(-8)	9.5000	1.791	-0.736
0.4880	1.456	-1.07(-8)	9.8000	2.128	-0.465
0.5145	1.454	-1.07(-8)	10.0000	2.094	-0.306
0.5500	1.454	-1.07(-8)	10.5910	1.805	-0.210
0.6328	1.452	-1.56(-8)	11.0000	1.823	-0.433
0.6943	1.452	-2.12(-8)	11.5000	2.024	-0.199
0.8600	1.448	-1.90(-7)	12.5000	1.808	-0.110
1.0600	1.443	-1.60(-6)	13.0000	1.790	-0.112
1.3000	1.432	-1.06(-5)	14.0000	1.739	-0.134
1.5360	1.425	-1.46(-4)	14.8000	1.663	-0.163
1.8000	1.411	-5.85(-4)	15.0000	1.656	-0.181
2.0000	1.405	-0.00134	16.4000	1.692	-0.463
2.2500	1.390	-0.00192	17.2000	2.003	-0.616
2.5000	1.362	-0.00399	18.0000	2.207	-0.166
2.7000	1.319	-0.00604	18.5000	2.041	-0.0940
3.0000	1.288	-0.0875	20.0000	1.895	-0.0558
3.2000	1.292	-0.144	21.3000	1.809	-0.146
3.3923	1.366	-0.178	22.5000	1.942	-0.187
3.5000	1.383	-0.179	25.0000	1.993	-0.0274
3.7500	1.420	-0.165	27.9000	1.916	-0.0221
4.0000	1.435	-0.151	30.0000	1.866	-0.0259
4.5000	1.427	-0.156	35.0000	1.856	-0.0315
5.0000	1.411	-0.137	40.0000	2.093	-0.131
5.5000	1.376	-0.195	50.0000	2.163	-0.238
6.0000	1.485	-0.195	60.0000	2.163	-0.263
6.2000	1.485	-0.147	80.0000	2.156	-0.276
6.5000	1.421	-0.0841	100.0000	2.173	-0.261
7.2000	1.235	-0.166	150.0000	2.183	-0.172
7.9000	1.148	-0.461	200.0000	2.176	-0.107
8.2000	1.220	-0.709	300.0000	2.179	-0.0386

4.2 The Proposed Background Stratospheric Aerosol Model

Figure 6 shows the extinction, scattering and absorption coefficients of the proposed background stratospheric aerosol model. Table 7 lists the values along with the asymmetry parameters. Figures 7 (a) to (d) compare the respective parameters against those developed by Shettle and Fenn[1] and used in LOWTRAN 6[2].

The extinction coefficients for the proposed model are smaller than those used of Shettle and Fenn. The differences are greatest for wavelengths longer than 10 μm. The differences are almost entirely due to changes in the absorption coefficient, as shown in Figure 7 (c). The differences in the scattering coefficients and asymmetry parameter are slight.

The changes seen in the proposed formulation are due almost entirely to the new indices of refraction. Figure 8 compares the extinction coefficients as a function of wavelength of the proposed model against those calculated using the proposed indices of refraction and the old modified gamma size distribution and against those calculated using the indices of refraction at 300 K and the proposed log normal size distribution. As shown, the change in indices of refraction is responsible for the majority of the difference.

4.2.1 Impact of Choice of Size Distribution

Based on our review of the literature (see Chapter 2) the size distribution that was chosen follows rec-

31

Table 7. Radiative Parameters for the Proposed Background Stratospheric Aerosol Model at 215 K. The numbers in parentheses are powers of ten

LAMBDA (μm)	INDEX OF REFRACTION n_r	n_i	EXTINCTION (km^{-1})	SCATTERING (km^{-1})	ABSORPTION (km^{-1})	SINGLE SCATTERING ALBEDO	ASYMMETRY PARAMETER
0.2000	1.526	0.0000	8.5042(-4)	8.5042(-4)	9.9774(-11)	1.000	0.6749
0.2500	1.512	0.0000	8.2526(-4)	8.2526(-4)	7.7618(-11)	1.000	0.6850
0.3000	1.496	0.0000	7.6454(-4)	7.6454(-4)	6.1260(-11)	1.000	0.6943
0.3371	1.48⁴	0.0000	7.0676(-4)	7.0676(-4)	5.3356(-11)	1.000	0.6991
0.4000	1.464	0.0000	5.9964(-4)	5.9964(-4)	4.2364(-11)	1.000	0.7038
0.4880	1.456	0.0000	4.7910(-4)	4.7910(-4)	3.2920(-11)	1.000	0.6944
0.5145	1.454	0.0000	4.4694(-4)	4.4694(-4)	3.0642(-11)	1.000	0.6910
0.5500	1.454	0.0000	4.0980(-4)	4.0980(-4)	2.8160(-11)	1.000	0.6846
0.6328	1.452	0.0000	3.3318(-4)	3.3318(-4)	3.4244(-11)	1.000	0.6694
0.6943	1.452	0.0000	2.8750(-4)	2.8750(-4)	4.1196(-11)	1.000	0.6572
0.8600	1.448	0.0000	1.9352(-4)	1.9352(-4)	2.7574(-10)	1.000	0.6251
1.0600	1.443	0.0000	1.2364(-4)	1.2363(-4)	1.7375(-9)	1.000	0.5861
1.3000	1.432	0.0000	7.3706(-5)	7.3696(-5)	8.6378(-9)	1.000	0.5405
1.5360	1.425	-0.0001	4.6880(-5)	4.6786(-5)	9.4560(-8)	0.998	0.4965
1.8000	1.411	-0.0006	2.8732(-5)	2.8426(-5)	3.0578(-7)	0.989	0.4499
2.0000	1.405	-0.0013	2.0992(-5)	2.0382(-5)	6.1016(-7)	0.971	0.4164
2.2500	1.390	-0.0019	1.4050(-5)	1.3297(-5)	7.5308(-7)	0.946	0.3772
2.5000	1.362	-0.0040	9.6202(-6)	8.2414(-6)	1.3788(-6)	0.857	0.3385
2.7000	1.319	-0.0060	6.9164(-6)	4.9962(-6)	1.9202(-6)	0.722	0.3069
3.0000	1.288	-0.0875	2.7254(-5)	2.9016(-6)	2.4352(-5)	0.106	0.2599
3.2000	1.292	-0.1440	3.9576(-5)	2.6414(-6)	3.6936(-5)	0.067	0.2352
3.3923	1.366	-0.1780	4.4846(-5)	3.3360(-6)	4.1510(-5)	0.074	0.2234
3.5000	1.383	-0.1790	4.3322(-5)	3.2514(-6)	4.0072(-5)	0.075	0.2165
3.7500	1.420	-0.1650	3.6740(-5)	2.9738(-6)	3.3766(-5)	0.081	0.2028
4.0000	1.435	-0.1510	3.1134(-5)	2.5120(-6)	2.8622(-5)	0.081	0.1878
4.5000	1.427	-0.1560	2.7706(-5)	1.6342(-6)	2.6072(-5)	0.059	0.1554
5.0000	1.411	-0.1370	2.1660(-5)	1.0347(-6)	2.0624(-5)	0.048	0.1291
5.5000	1.376	-0.1950	2.7660(-5)	6.9628(-7)	2.6964(-5)	0.025	0.1057
6.0000	1.485	-0.1950	2.3758(-5)	7.4808(-7)	2.3010(-5)	0.031	0.0962
6.2000	1.485	-0.1470	1.7405(-5)	6.2782(-7)	1.6777(-5)	0.036	0.0909
6.5000	1.421	-0.0841	9.9074(-6)	3.8906(-7)	9.5182(-6)	0.039	0.0802
7.2000	1.235	-0.1660	1.8893(-5)	1.2362(-7)	1.8769(-5)	0.007	0.0595
7.9000	1.148	-0.4610	5.0566(-5)	2.5844(-7)	5.0306(-5)	0.005	0.0458
8.2000	1.220	-0.7090	7.2532(-5)	5.4006(-7)	7.1992(-5)	0.007	0.0413
8.5000	1.457	-0.8400	6.8040(-5)	6.9298(-7)	6.7348(-5)	0.010	0.0418
8.7000	1.753	-0.8170	5.0772(-5)	7.0854(-7)	5.0062(-5)	0.014	0.0479
9.0000	1.767	-0.6040	3.6972(-5)	4.7534(-7)	3.6496(-5)	0.013	0.0483
9.2000	1.704	-0.5570	3.5158(-5)	3.8212(-7)	3.4776(-5)	0.011	0.0451
9.5000	1.791	-0.7360	4.0840(-5)	4.6384(-7)	4.0378(-5)	0.011	0.0425
9.8000	2.128	-0.4650	1.9955(-5)	4.3004(-7)	1.9525(-5)	0.022	0.0525
10.0000	2.094	-0.3060	1.3457(-5)	3.5238(-7)	1.3105(-5)	0.026	0.0504
10.5910	1.805	-0.2100	1.0871(-5)	1.7696(-7)	1.0694(-6)	0.016	0.0379
11.0000	1.823	-0.4330	2.0778(-5)	1.8759(-7)	2.0590(-5)	0.009	0.0346
11.5000	2.024	-0.1990	7.9792(-6)	1.7553(-7)	7.8036(-6)	0.022	0.0365
12.5000	1.808	-0.1100	4.7986(-6)	8.6996(-8)	4.7116(-6)	0.018	0.0273
13.0000	1.790	-0.1120	4.7434(-6)	7.1830(-8)	4.6716(-6)	0.015	0.0250
14.0000	1.739	-0.1340	5.4362(-6)	4.8632(-8)	5.3876(-6)	0.009	0.0209
14.8000	1.663	-0.1630	6.6002(-6)	3.3622(-8)	6.5666(-6)	0.005	0.0180
15.0000	1.656	-0.1810	7.2602(-6)	3.1790(-8)	7.2284(-6)	0.004	0.0174
16.4000	1.692	-0.4630	1.6200(-5)	3.2838(-8)	1.6168(-5)	0.002	0.0144
17.2000	2.003	-0.6160	1.5554(-5)	4.4028(-8)	1.5510(-5)	0.003	0.0151
18.0000	2.207	-0.1660	3.5504(-6)	3.4570(-8)	3.5158(-6)	0.010	0.0163
18.5000	2.041	-0.0940	2.2486(-6)	2.5334(-8)	2.2232(-6)	0.011	0.0141
20.0000	1.895	-0.0558	1.3897(-6)	1.4947(-8)	1.3747(-6)	0.011	0.0111
21.3000	1.809	-0.1460	3.6235(-6)	1.0301(-8)	3.6128(-6)	0.003	0.0094

Table 7.   (Cont.)

LAMBDA (μm)	INDEX OF REFRACTION n_r	n_i	EXTINCTION (km^{-1})	SCATTERING (km^{-1})	ABSORPTION (km^{-1})	SINGLE SCATTERING ALBEDO	ASYMMETRY PARAMETER
22.5000	1.942	-0.1870	3.9294(-6)	1.0351(-8)	3.9190(-6)	0.003	0.0090
25.0000	1.993	-0.0274	5.0360(-7)	7.0124(-9)	4.9658(-7)	0.014	0.0075
27.9000	1.916	-0.0221	3.8602(-7)	4.0356(-9)	3.8198(-7)	0.010	0.0058
30.0000	1.866	-0.0259	4.3630(-7)	2.7856(-9)	4.3352(-7)	0.006	0.0049
35.0000	1.856	-0.0315	4.5664(-7)	1.4768(-9)	4.5516(-7)	0.003	0.0036
40.0000	2.093	-0.1310	1.3585(-6)	1.2212(-9)	1.3573(-6)	0.001	0.0031
50.0000	2.163	-0.2380	1.8508(-6)	5.5384(-10)	1.8503(-6)	0.000	0.0020
60.0000	2.163	-0.2630	1.7005(-6)	2.6910(-10)	1.7002(-6)	0.000	0.0014
80.0000	2.156	-0.2760	1.3442(-6)	8.4884(-11)	1.3441(-6)	0.000	0.0008
100.0000	2.173	-0.2610	1.0032(-6)	3.5132(-11)	1.0032(-6)	0.000	0.0005
150.0000	2.183	-0.1720	4.3904(-7)	6.8248(-12)	4.3902(-7)	0.000	0.0002
200.0000	2.176	-0.1070	2.0646(-7)	2.1174(-12)	2.0646(-7)	0.000	0.0001
300.0000	2.179	-0.0386	4.9588(-8)	4.1658(-13)	4.9588(-8)	0.000	0.0001
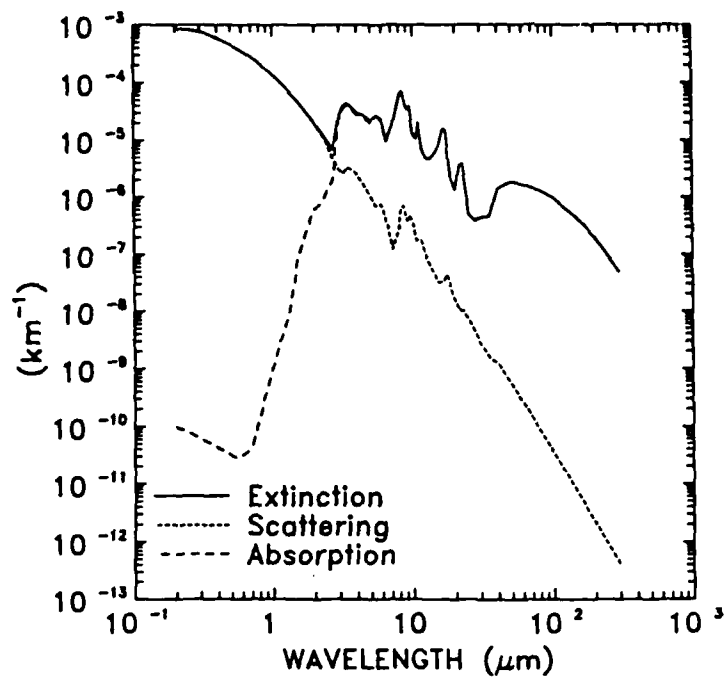
Figure 6. Extinction, Scattering and Absorption
Coefficients as a Function of Wavelength for the Proposed
Background Stratospheric Aerosol Model
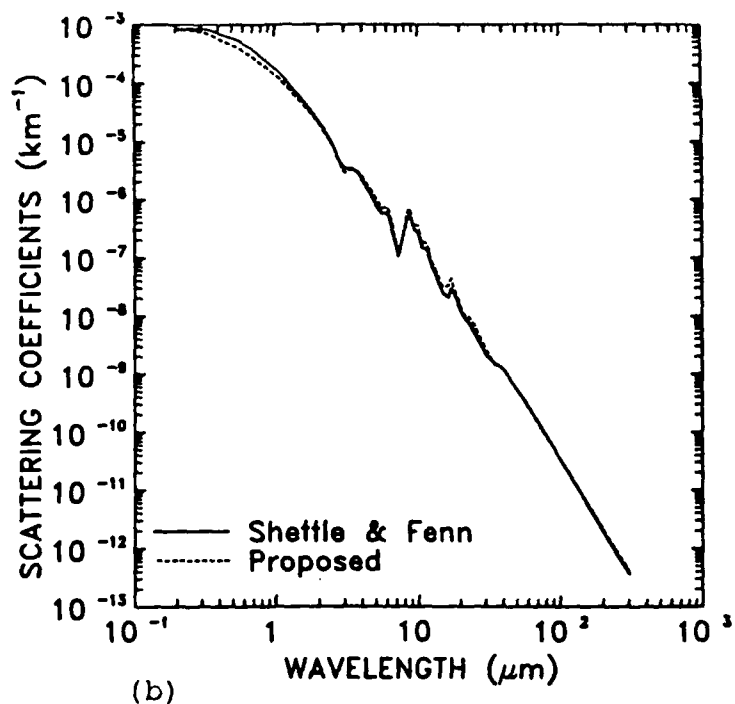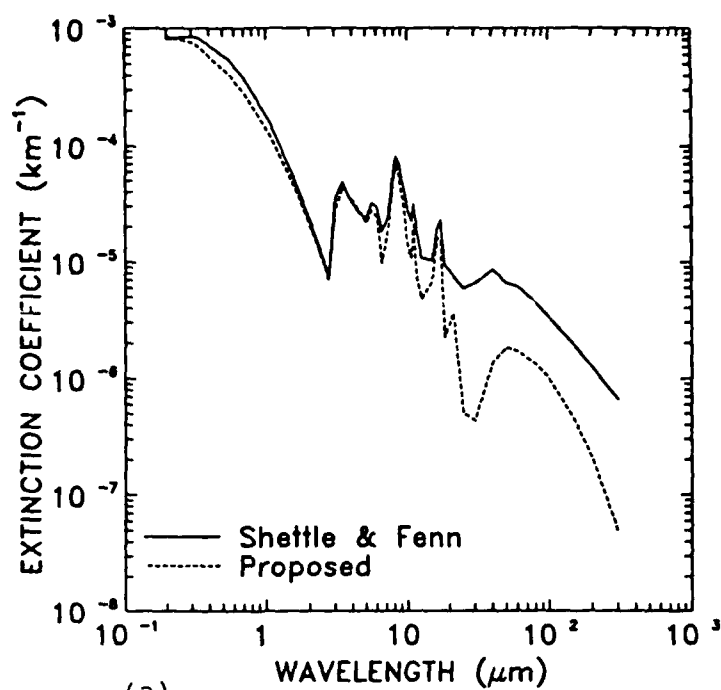
Figure 7. Comparison of the Proposed Background
Stratospheric Aerosol Model and that in Shettle and Fenn (a)
Extinction Coefficients, (b) Scattering Coefficients, (c)
Absorption Coefficients, and (d) Asymmetry Parameter
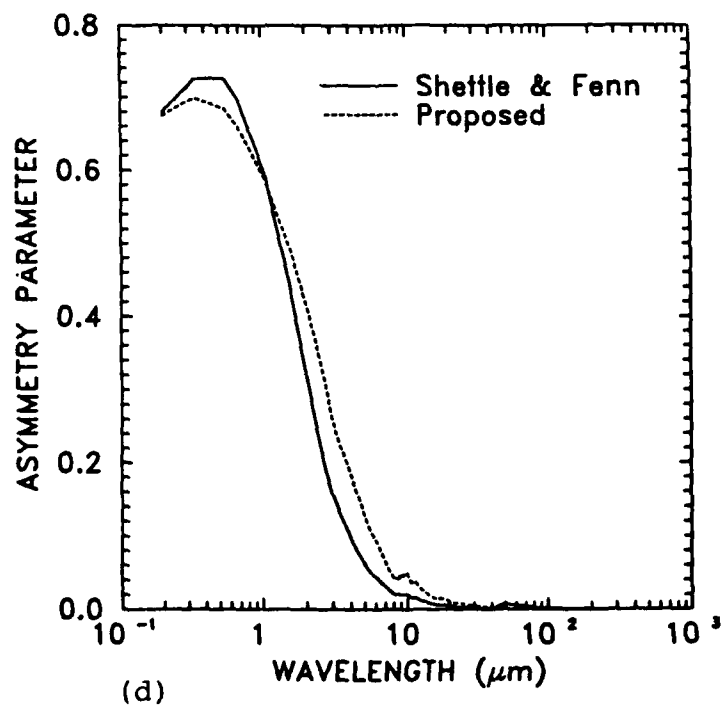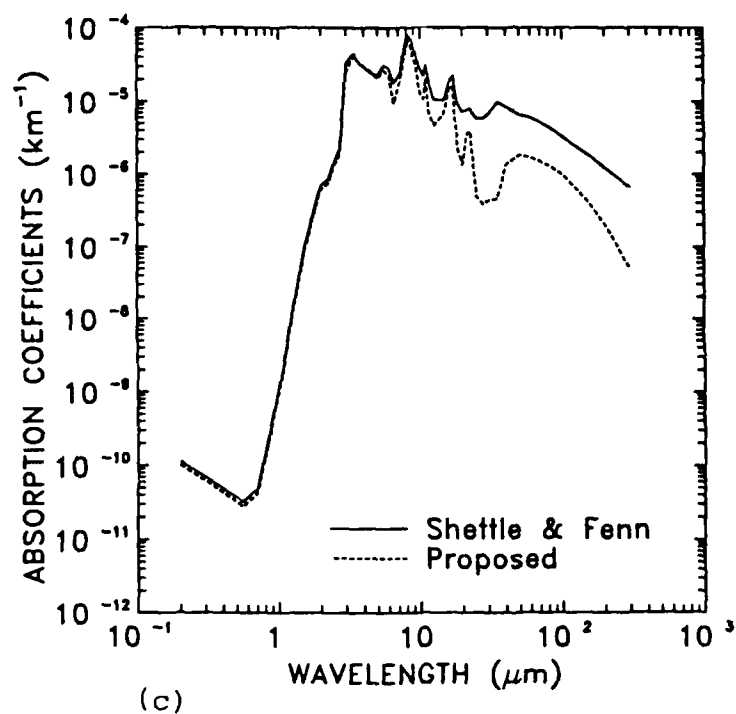
Figure 7. (c) and (d) (continued)
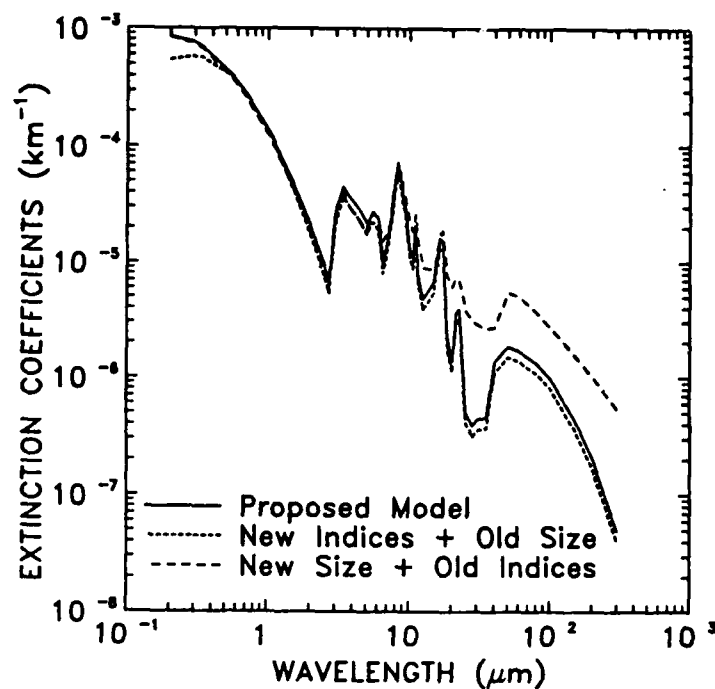
Figure 8. Extinction Coefficients as a Function of
Wavelength for the Proposed Model (Solid Line), Calculated
Using the Proposed Indices of Refraction and the Modified
Gamma Size Distribution (Dotted Line) and Calculated Using
the Indices of Refraction at 300 K and the Proposed Log
Normal Size Distribution

ommendations from the meeting of experts held by the World Meteorological Organization[10]. Other sets of log normal parameters have been suggested by other researchers and Figure 9 compares the extinction coefficients as a function of wavelength calculated with the proposed size distribution against those calculated by other suggested size distributions. The indices of refraction at 215 K were used in all cases.
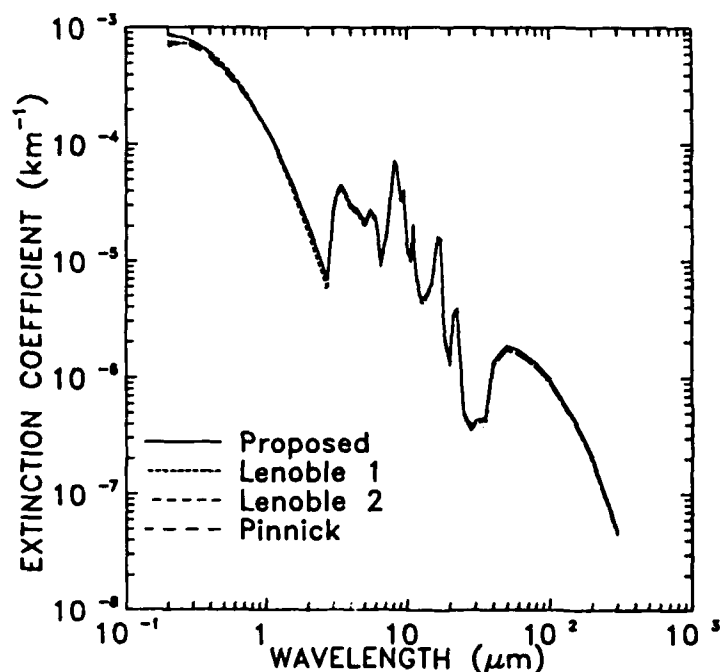
Figure 9. Extinction Coefficients as a Function of Wavelength for the Proposed Model and for Three Alternative Size Distributions

The values of the parameters for the log normal distribution are listed in Table 8. The particle number densities were scaled so as to produce an extinction coefficient of 1.2×10^{-4} km^{-1} at 1.0 μm. The curves labled Lenoble 1 and 2 are from the work of Brogniez and Lenoble[38] and the curve labled Pinnick is from Pinnick et al.[26]. The curves are es-

Table 8. Values of Log Normal Size Distribution Parameters in Eq. (7) for the Different Stratospheric Models Compared in Figure 9. The N_o values have been normalized to produce an extinction coefficient of 1.2×10^{-4} km^{-1} at the wavelength 1.0 µm

CURVE	N_o ($\# \ cm^{-3}$)	R (µm)	σ
Proposed	9.0	0.0695	1.86
Lenoble 1	3.3	0.12	1.604
Lenoble 2	11.7	0.06	1.919
Pinnick	7.4	0.0725	1.86

sentially the same, as shown in Figure 10 which shows the ratios of the extinction coefficients shown in Figure 9 to the proposed values, leading one to draw the conclusion that the choice of parameters for the log normal distribution has little impact on the resultant extinction coefficients.

4.2.2 Impact of Choice of Stratospheric Temperature

The value of 215 K was chosen to be representative of stratospheric conditions in an annually averaged, mid-latitude atmosphere. The impact of using these values for other latitudes or seasons can be demonstrated in Figure 11 which shows extinction coefficients at 250 K and 180 K. The values at 250 K are greater for the far infrared wavelengths as a result of the larger imaginary component (see Appendix A). Conversely, the lower imaginary components at 180 K are reflected as lower extinction coefficients at the far infrared wavelengths. The values of the attenuation coefficients for the extreme stratospheric temperatures of 180 and 250 K are tabulated in the Appendix for reference.
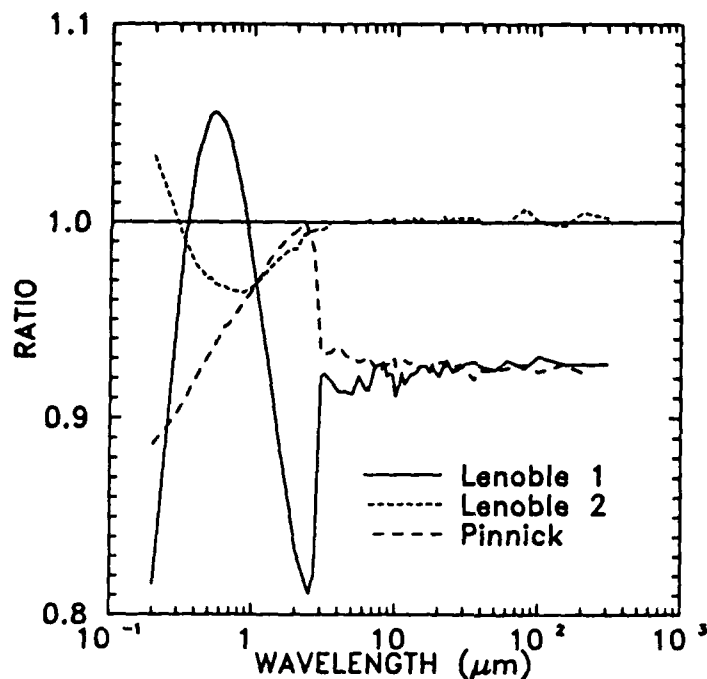
Figure 10. Ratios of the Extinction Coefficients Shown in Figure 9 to the Proposed Formulation as a Function of Wavelength
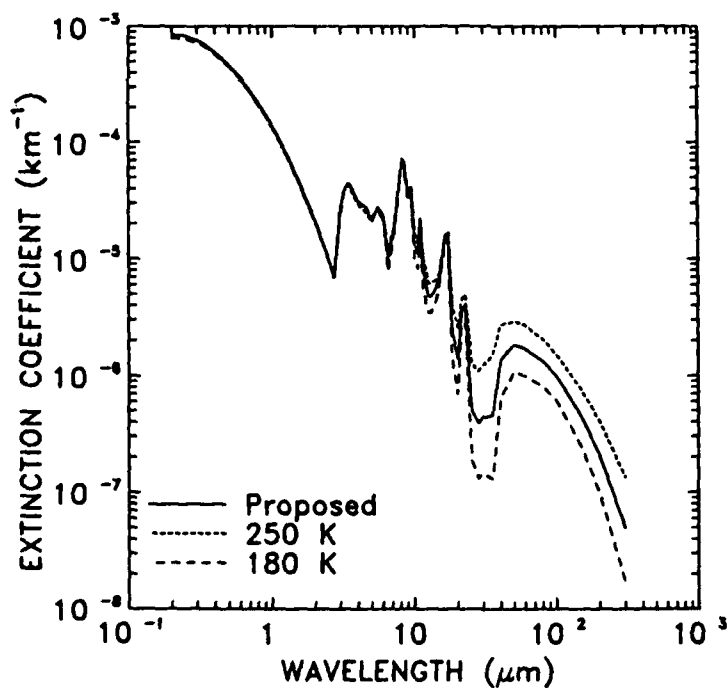
Figure 11. Extinction Coefficients as a Function of Wavelength for the Proposed Model (and Assumed Stratospheric Temperature of 215 K) and With Indices of Refraction Calculated for 180 K and 250 K

4.3 Enhanced Aerosols After a Volcanic Eruption

A volcanic eruption will increase the numbers and size distribution of sulfuric acid particles as a result of SO_2 injections into the stratosphere. The specific impact on aerosol loadings in terms of size distribution and mixture of H_2SO_4 and water will vary from eruption to eruption.

Figure 12 shows the extinction coefficients for stratospheric aerosols that have been "enhanced" by the chemical production and sedimentation of sulfuric acid particles. The calculations were based on the sum of two log normal size distributions based upon the work of Oberbeck et al.[29] following the eruption of El Chichon. The first distribution represents an enhanced background and has a particle
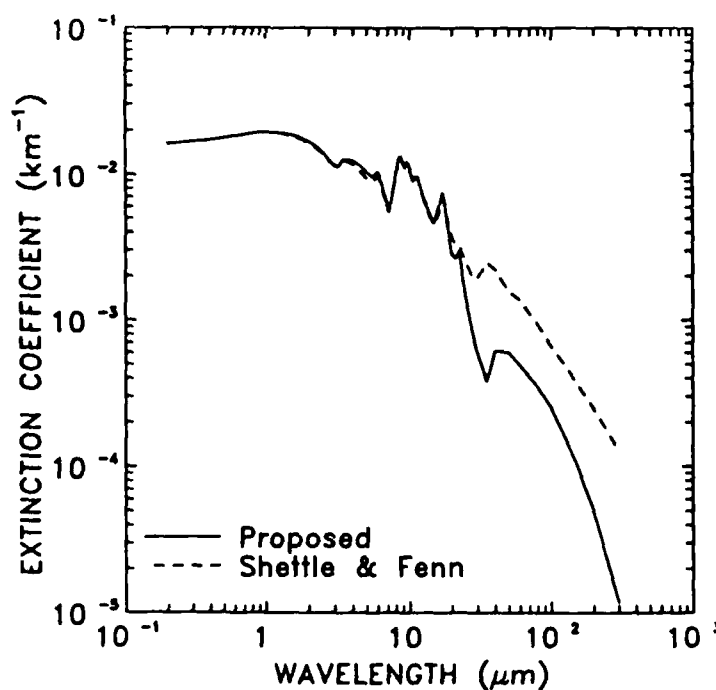
Figure 12. Extinction Coefficients as a Function of Wavelength for a Postulated Enhanced Stratospheric Aerosol Layer

density of 6 cm^{-3}, mode radius of 0.14 µm and standard deviation of 1.72 (e.g. Eq. (7)). The second distribution results from the sedimentation of smaller particles and is represented by a particle density of 1.5 cm^{-3}, a mode radius of 0.54 µm and a standard deviation of 1.22. The calculations were done with the proposed indices of refraction at 215 K and those at 300 K.

Both curves show a nearly flat response as a function of wavelength up to about 1.0 µm. Significant differences between the curves do not begin to appear until beyond 20 µm as a result of the differences in the imaginary component of the indices of refraction.

5. CONCLUSIONS AND RECOMMENDATIONS

5.1 Conclusions

A new background stratospheric aerosol model for use in LOWTRAN 7[44] has been developed. The new model is intended to replace the background stratospheric aerosol model formulation currently in use in LOWTRAN 6[2] that is based on indices of refraction for sulfuric acid droplets at 300 K. The new model includes indices of refraction for a mixture of 75 % H_2SO_4 and 25 % H_2O at temperatures representative of a mean stratosphere (215 K) and a log normal size distribution that is consistent with observations. Indices of refraction at temperatures between 150 and 300 K have also been calculated.

The extinction coefficients for the proposed model are smaller than those used in LOWTRAN 6. The differences are greatest for wavelengths longer than 10 μm. The differences are almost entirely due to changes in the absorption coefficient as a result of smaller imaginary components of the index of refraction at these wavelength.

5.1.1 Impact of Choice of Size Distribution

There is little impact from the change from a modified gamma to a log normal size distribution. In addition, the choice of parameters for the log normal size distribution has little impact on the extinction coefficients.

44. Kneizys, F.X., Shettle, E.P., Abreu, L.W., Chetwynd, J.H., Anderson, G.P., Gallery, W.O., Selby, J.E.A., and Clough, S.A. (1988) Users Guide to LOWTRAN 7, AFGL-TR-88-0177, Air Force Geophysics Laboratory, Hanscom AFB, Massachusetts, 16 August 1988. ADA206773

5.1.2 Impact of Choice of Representative Stratospheric Temperature

The value of 215 K was chosen to be representative of stratospheric conditions in an annually averaged, mid-latitude atmosphere. Examples of extinction coefficients determined for indices of refraction representative of extreme stratospheric conditions have also been presented.

5.2 Recommendations for Future Research

A single set of radiative parameters for the proposed background stratospheric aerosol model have been calculated in order to simplify its inclusion in LOWTRAN 7[44]. While the temperature chosen is more representative of temperatures found in the stratosphere, it would not correctly represent conditions found at low or high latitudes or be representative of seasonal changes.

Values of the indices of refraction for H_2SO_4 at temperatures representative of the full range of stratospheric temperatures were also calculated. These indices of refraction could be coupled to a temperature dependent radiation model in which the radiative parameters are coupled to a mean temperature inputed for the stratosphere by the user.

1. Shettle, E. P. and R. W. Fenn (1976) "Models of the Atmospheric Aerosols and Their Optical Properties," in AGARD Conference Proceedings No. 183, Optical Propagation in the Atmosphere. Presented at the Electromagnetic Wave Propagation Panel Symposium, Lyngby, Denmark, 27-31 October 1975, AGARD-CP-183, ADA028-615.

2. Kneizys, F. X., Shettle, E. P., Gallery, W. O., Chetwynd, J. H., Abreu, L. W., Selby, J. E. A., Clough, S. A., and Fenn, R. W. (1983) Atmospheric transmittance/radiance: Computer code LOWTRAN 6, AFGL-TR-83-0187, AD 137796.

3. Clough, S. A., Kneizys, F. X., Shettle, E. P., and Anderson, G. P. (1986) Atmospheric radiance and transmittance: FASCOD2, Proceedings of the Sixth Conference on Atmospheric Radiation, Williamsburg, Virginia, American Meteorological Society, Boston, Massachusetts, 141-144.

4. WCP (1986) A preliminary cloudless standard atmosphere for radiation computation, WCP-112, WMO/TD-No 24, World Climate Research Programme, International Association of Meteorology and Atmospheric Physics/Radiation Commission.

5. Remsberg, E. E. (1971) Radiative properties of several probable constituents of Atmospheric Aerosols, PhD. Thesis, Department of Meteorology, University of Wisconsin, Madison.

6. Remsberg, E. E. (1973) Stratospheric aerosol properties and their effects on infrared radiation, J. Geophys. Res., 78:1401-1407.

7. Palmer, K. F. and D. Williams (1975) Optical constants of sulfuric acid; Application to the clouds of Venus?. Applied Optics, 14:208-219.

8. Volz, F. E. (1973) Infrared optical constants of ammonium sulfate, Sahara dust, volcanic pumice, and flyash, Appl. Opt., 12:564-568.

9. Pinkley, L. W. and Williams, D. (1976) The infrared optical constants of sulfuric acid at 250 K, J. Opt. Soc. Am., 66:122-124.

10. WCP (1983) <u>Report of the Experts Meeting on Aerosols and Their Climatic Effects</u>, Eds. Deepak, A. and Gerber, H. E., World Climate Programme, WCP 55, World Meteorological Organization, p 30.

11. Reiter, R., Jager, H., Carmuth, W., and Funk, W. (1979) The stratospheric aerosol layer observed by lidar since October 1976. A contribution to the problem of hemispheric climate, <u>Arch. Met. Geoph. Biokl.</u>, <u>Ser. B</u>, <u>27</u>:121-149.

12. D'Altorio, A., Viconti, G., and Fiocco, G. (1981) Lidar detection of volcanic aerosols in the atmosphere following the Mount St. Helen eruption, <u>Geophys. Res. Let.</u>, <u>8</u>:63-65.

13. Clemesha, B. R. and Simmonich, D. M. (1978) Stratospheric dust measurements, 1970-1977, <u>J. Geophys. Res.</u>, <u>83</u>:2403-2408.

14. Iwasaka, Y., Hayashida, S., and Cno, A. (1983) Increasing backscattered light from the stratospheric aerosol layer radar after Mt. El Chichon eruption, laser radar Measurement at Nagoya (35°N, 137°E), <u>Geophys. Res. Let.</u>, <u>6</u>:440-442.

15. Hirono, M., Fujiwara, M., Shibata, T., and Kugumiya, N. (1981) Lidar observations of Mt. St. Helens in May 1980, <u>Geophys. Res. Let.</u>, <u>9</u>:1019-1022.

16. McCormick, M. P., Swissler, T. J. (1983) Stratospheric aerosol mass and latitudinal distribution of the El Chicon eruption cloud for October 1982, <u>Geophys. Res. Let.</u>, <u>9</u>:877-880.

17. Clemesha, B. R. and Simonich, D. M (1983) Lidar observations of the El Chicon dust cloud at 23°S, <u>Geophys. Res. Let.</u>, <u>10</u>:321-324.

18. Hirono, M., Fujiwara, M.,and Shibata, T. (1981) Lidar observation of sudden increases of aerosols in the stratosphere caused by volcanic injections. I. Soufriere 1979 event, <u>J. Atmos. Terr. Phy</u>, <u>43</u>:1127-1131.

19. Hirono, M., Fujiwara, M.,and Shibata, T. (1982) Lidar observation of sudden increases of aerosols in the stratosphere caused by volcanic injections. II. Sierra Negra event, <u>J. Atmos. Terr. Phy</u>, <u>44</u>:811-818.

20. Hirono, M. and Shibata, T. (1983) Enormous increase of stratospheric aerosols over Fukuoro due to volcanic eruption of El Chicon in 1982, Geophys. Res. Let., 10: 152-154.

21. D'Altorio, A. and Visconti, G. (1983) Lidar observations of dust layers' transience in the stratosphere following the El Chichon volcanic eruption, Geophys. Res. Let., 10:27-30.

22. Rosen, J. M., Hofmann, D. J., and Laby, J., (1975) Stratospheric aerosol measurements, II, Worldwide distribution, J. Atmos. Sci., 32:1457-1462.

23. Hofmann, D. J., and Rosen, J. M., (1982) Balloon-borne observations of stratospheric aerosol and condensation nuclei during the year following the Mt. St. Helens Eruption, J. Geophys. Res., 87:11039-11061.

24. Hofmann, D. J., and Rosen, J. M., (1983) Stratospheric sulfuric acid fraction and mass estimate for the 1982 volcanic eruption at El Chichon, Geophys. Res. Let, 10:313-316.

25. Hofmann, D. J., and Rosen, J. M., (1984) On the temporal variation of stratospheric aerosol size and mass during the first 18 months following the 1982 eruption of El Chichon, J. Geophys. Res., 89:4883-4890.

26. Pinnick, R. G., Rosen, J. M., and Hofmann, D. J., (1976) Stratospheric aerosol measurements, III, Optical model measurements, J. Atmos. Sci., 33:304-314.

27. Oberbeck, V. R., Farlow. N. H., Fong, W., Snetsinger, K. G., Ferry, G. V. Ferry and Hayes, D. M., (1982) Mount St. Helens aerosol evolution, Geophys. Res. Let., 9:1089-1092.

28. Knollenberg, R. G., and Huffmann, D., (1983) Measurements of the aerosol size distributions in the El Chichon cloud, Geophys. Res. Let., 10:1025-1028.

29. Oberbeck, V. R., Danielsen, E. F., Snetsinger, K. G., Ferry, G. V. Fong, W., Hayes, D. M., (1983) Effect of the eruption of El Chichon on stratospheric aerosol size and composition, Geophys. Res. Let., 10:1021-1024.

30. Wilson, J. C., Blackshear, E. D., and Hyun, J. H., (1983) Changes in the sub-2.5 micron diameter aerosol observed at 20 km altitude after the eruption of El Chichon, Geophys. Res. Let., 10:1029-1032.

31. Witteborn, F. C., O'Brien, K., Crean, H. W. Pollack, J. B., and Bilski, K. H., (1983) Spectroscopic measurements of the 8- to 13-micrometer transmission of the upper atmosphere following the El Chichon eruptions, Geophys. Res. Let., 10:1009-1012.

32. Dutton, E., and DeLuisi, J., (1983) Extinction of solar radiation by the El Chichon dust cloud, Geophys. Res. Let., 10:1013-1016.

33. Woods, D. C., and Chuan, R. L., (1983) Size-specific compositions of aerosols in the El Chichon volcanic cloud, Geophys. Res. Let., 10:1041-1044.

34. Patterson, E. M. (1981) Measurements of the imaginary part of the refractive index between 300 and 700 nanometers for Mount St. Helens ash, Science, 211:836-838.

35. Patterson, E. M., Pollard, C. O., and Galindo, I., (1983) Optical properties of the ash from El Chichon, Geophys. Res. Let., 10:317-320.

36. Russell, P. B., McCormick, M. P.,Swissler, T. J. Chu, W.P., Livingston, J. M., Fuller, W. H , Rosen, J. M., Hofmann, D. J., McMaster, L. R., Woods, D. C. and Pepin, T. J. (1981) Satellite and correlative measurements of the stratospheric aerosol. II: Comparison of measurements made by SAM II, dust-sondes and an airborne Lidar, J. Atmos. Sci., 38: 1295-1312.

37. Lenoble. J., Pruvost, P. and Brogniez, C. (1984) SAGE satellite observations of stratospheric aerosols from Mount St. Helens eruption: A two-wavelength analysis, J. Geophys. Res., 89:11666-11676.

38. Brogniez, C., and Lenoble, J., (1987) Modeling of the stratospheric background aerosols from zonally averaged SAGE profiles, J. Geophys. Res., 92:3051-3060.

39. Jackson, J. D. (1975) Classical Electrodynamics, John Wiley & Sons, 2 nd Edition, New York, p 155.

40. Mayer, J. E., and Mayer, M. G. (1940) Statistical Mechanics, John Wiley & Sons, New York, p 340.

41. Roth, W. A. and Scheel,K., eds. (1923) <u>Landolt-Born-stein Physikalisch-Chemische Tabellen</u>, Verlag von Julius, Springer, Berlin, 397-398.

42. Jones, A. D. (1976) Optical constants of sulfuric acid in the far infrared, <u>J. Quant. Spectrosc. Radiat. Transfer</u>, <u>16</u>:1017-1019.

43. Rossow, W. B., and Sagan, C., (1975) Microwave boundary conditions on the atmosphere and clouds of Venus, <u>J. Atmos. Sci.</u>, <u>32</u>:1164-1176.

44. Kneizys, F.X., Shettle, E.P., Abreu, L.W., Chetwynd, J.H., Anderson, G.P., Gallery, W.O., Selby, J.E.A., and Clough, S.A. (1988) <u>Users Guide to LOWTRAN 7</u>, AFGL-TR-88-0177, Air Force Geophysics Laboratory, Hanscom AFB, Massachusetts, 16 August 1988.ADA206773

Temperature Dependent Indices of Refraction and Radiative Properties for the Background Stratospheric Model

Table A-1 lists the temperature dependent indices of refraction for sulfuric acid and water for the temperature range from 150 to 300 K. Table A-2 lists the radiative properties for the background stratospheric model at 180 K and Table A-3 lists the properties at 250 K.

Table A-1. Temperature Dependent Real, n_r, and Imaginary, n_i, Indices of Refraction for a 75% Solution of H_2SO_4 and Water. The numbers in parentheses are powers of ten

LAMBDA	300 K		290 K		280 K		270 K	
(μm)	n_r	n_i	n_r	n_i	n_r	n_i	n_r	n_i
0.2000	1.498	-1.00(-8)	1.501	-1.01(-8)	1.505	-1.02(-8)	1.508	-1.02(-8)
0.2500	1.484	-1.00(-8)	1.487	-1.01(-8)	1.490	-1.02(-8)	1.494	-1.02(-8)
0.3000	1.469	-1.00(-8)	1.472	-1.01(-8)	1.475	-1.02(-8)	1.478	-1.02(-8)
0.3371	1.459	-1.00(-8)	1.462	-1.01(-8)	1.465	-1.02(-8)	1.468	-1.02(-8)
0.4000	1.440	-1.00(-8)	1.443	-1.01(-8)	1.446	-1.02(-8)	1.449	-1.02(-8)
0.4880	1.432	-1.00(-8)	1.435	-1.01(-8)	1.438	-1.02(-8)	1.441	-1.02(-8)
0.5145	1.431	-1.00(-8)	1.434	-1.01(-8)	1.437	-1.02(-8)	1.439	-1.02(-8)
0.5500	1.430	-1.00(-8)	1.433	-1.01(-8)	1.435	-1.02(-8)	1.438	-1.02(-8)
0.6328	1.429	-1.47(-8)	1.432	-1.48(-8)	1.434	-1.49(-8)	1.437	-1.50(-8)
0.6943	1.428	-1.99(-8)	1.431	-2.00(-8)	1.433	-2.02(-8)	1.436	-2.04(-8)
0.8600	1.425	-1.79(-7)	1.428	-1.80(-7)	1.430	-1.82(-7)	1.433	-1.83(-7)
1.0600	1.420	-1.50(-6)	1.423	-1.51(-6)	1.425	-1.52(-6)	1.428	-1.53(-6)
1.3000	1.410	-1.00(-5)	1.413	-1.01(-5)	1.415	-1.01(-5)	1.418	-1.02(-5)
1.5360	1.403	-1.37(-4)	1.405	-1.38(-4)	1.408	-1.39(-4)	1.411	-1.40(-4)
1.8000	1.390	-5.50(-4)	1.392	-5.54(-4)	1.395	-5.58(-4)	1.398	-5.62(-4)
2.0000	1.384	-0.00126	1.386	-0.00127	1.389	-0.00128	1.391	-0.00129
2.2500	1.370	-0.00180	1.372	-0.00181	1.375	-0.00183	1.377	-0.00184
2.5000	1.344	-0.00376	1.346	-0.00379	1.348	-0.00381	1.351	-0.00384
2.7000	1.303	-0.00570	1.305	-0.00574	1.307	-0.00578	1.309	-0.00582
3.0000	1.293	-0.0955	1.292	-0.0945	1.292	-0.0936	1.291	-0.0926
3.2000	1.311	-0.135	1.309	-0.136	1.307	-0.137	1.304	-0.138
3.3923	1.352	-0.159	1.354	-0.161	1.355	-0.163	1.357	-0.166
3.5000	1.376	-0.158	1.377	-0.160	1.378	-0.163	1.378	-0.165
3.7500	1.396	-0.131	1.399	-0.135	1.402	-0.138	1.404	-0.142
4.0000	1.398	-0.126	1.402	-0.129	1.407	-0.131	1.411	-0.134
4.5000	1.385	-0.120	1.390	-0.124	1.395	-0.128	1.400	-0.132
5.0000	1.360	-0.121	1.366	-0.123	1.372	-0.125	1.378	-0.126
5.5000	1.337	-0.183	1.342	-0.184	1.346	-0.186	1.351	-0.187
6.0000	1.425	-0.195	1.432	-0.195	1.439	-0.195	1.446	-0.195
6.2000	1.424	-0.165	1.431	-0.163	1.438	-0.161	1.446	-0.158
6.5000	1.370	-0.128	1.376	-0.122	1.382	-0.116	1.388	-0.110
7.2000	1.210	-0.176	1.213	-0.175	1.216	-0.174	1.219	-0.172
7.9000	1.140	-0.488	1.141	-0.485	1.142	-0.482	1.143	-0.478
8.2000	1.200	-0.645	1.202	-0.652	1.205	-0.660	1.207	-0.667
8.5000	1.370	-0.755	1.380	-0.765	1.390	-0.774	1.401	-0.784
8.7000	1.530	-0.772	1.556	-0.777	1.582	-0.782	1.609	-0.787
9.0000	1.650	-0.633	1.664	-0.630	1.678	-0.626	1.691	-0.623
9.2000	1.600	-0.586	1.612	-0.583	1.624	-0.579	1.637	-0.576
9.5000	1.670	-0.750	1.684	-0.748	1.698	-0.747	1.713	-0.745
9.8000	1.910	-0.680	1.936	-0.650	1.961	-0.622	1.987	-0.595
10.0000	1.890	-0.455	1.914	-0.434	1.938	-0.414	1.962	-0.395
10.5910	1.720	-0.340	1.730	-0.321	1.740	-0.304	1.750	-0.287
11.0000	1.670	-0.485	1.688	-0.479	1.706	-0.472	1.724	-0.466
11.5000	1.890	-0.374	1.906	-0.347	1.922	-0.322	1.937	-0.299
12.5000	1.740	-0.198	1.748	-0.185	1.756	-0.172	1.764	-0.161
13.0000	1.690	-0.195	1.702	-0.183	1.714	-0.171	1.725	-0.161
14.0000	1.640	-0.195	1.652	-0.187	1.663	-0.178	1.675	-0.171
14.8000	1.610	-0.205	1.616	-0.200	1.622	-0.194	1.629	-0.189
15.0000	1.590	-0.211	1.598	-0.207	1.606	-0.204	1.613	-0.200
16.4000	1.520	-0.414	1.540	-0.419	1.560	-0.425	1.581	-0.431
17.2000	1.724	-0.590	1.757	-0.593	1.790	-0.596	1.822	-0.599
18.0000	1.950	-0.410	1.980	-0.369	2.010	-0.331	2.041	-0.298
18.5000	1.927	-0.302	1.940	-0.263	1.954	-0.229	1.967	-0.200

Table A-1. (Cont.)

LAMBDA (μm)	300 K n_r	n_i	290 K n_r	n_i	280 K n_r	n_i	270 K n_r	n_i
20.0000	1.810	-0.230	1.820	-0.195	1.830	-0.165	1.840	-0.140
21.3000	1.790	-0.250	1.792	-0.235	1.794	-0.220	1.797	-0.207
22.5000	1.820	-0.290	1.834	-0.275	1.849	-0.262	1.863	-0.248
25.0000	1.840	-0.240	1.858	-0.186	1.876	-0.144	1.894	-0.112
27.9000	1.780	-0.250	1.796	-0.188	1.812	-0.141	1.828	-0.106
30.0000	1.730	-0.290	1.746	-0.218	1.762	-0.164	1.778	-0.124
35.0000	1.720	-0.520	1.736	-0.374	1.752	-0.269	1.768	-0.193
40.0000	1.940	-0.630	1.958	-0.524	1.976	-0.435	1.994	-0.362
50.0000	2.010	-0.650	2.028	-0.578	2.046	-0.513	2.064	-0.456
60.0000	2.010	-0.730	2.028	-0.647	2.046	-0.574	2.064	-0.509
80.0000	2.020	-0.720	2.036	-0.643	2.052	-0.575	2.068	-0.514
100.0000	2.020	-0.650	2.038	-0.584	2.056	-0.524	2.074	-0.471
150.0000	2.030	-0.560	2.048	-0.488	2.066	-0.424	2.084	-0.369
200.0000	2.040	-0.490	2.056	-0.410	2.072	-0.342	2.088	-0.286
300.0000	2.060	-0.390	2.074	-0.297	2.088	-0.226	2.102	-0.172

Table A-1. (Cont.)

LAMBDA (µm)	260 K n_r	260 K n_i	250 K n_r	250 K n_i	240 K n_r	240 K n_i	230 K n_r	230 K n_i
0.2000	1.511	-1.03(-8)	1.515	-1.04(-8)	1.518	-1.05(-8)	1.521	-1.06(-8)
0.2500	1.497	-1.03(-8)	1.500	-1.04(-8)	1.503	-1.05(-8)	1.507	-1.06(-8)
0.3000	1.481	-1.03(-8)	1.484	-1.04(-8)	1.488	-1.05(-8)	1.491	-1.06(-8)
0.3371	1.471	-1.03(-8)	1.474	-1.04(-8)	1.477	-1.05(-8)	1.480	-1.06(-8)
0.4000	1.451	-1.03(-8)	1.454	-1.04(-8)	1.457	-1.05(-8)	1.460	-1.05(-8)
0.4880	1.443	-1.03(-8)	1.446	-1.04(-8)	1.449	-1.05(-8)	1.452	-1.05(-8)
0.5145	1.442	-1.03(-8)	1.445	-1.04(-8)	1.448	-1.05(-8)	1.451	-1.05(-8)
0.5500	1.441	-1.03(-8)	1.444	-1.04(-8)	1.447	-1.05(-8)	1.450	-1.05(-8)
0.6328	1.440	-1.52(-8)	1.443	-1.53(-8)	1.446	-1.54(-8)	1.448	-1.55(-8)
0.6943	1.439	-2.05(-8)	1.442	-2.07(-8)	1.445	-2.08(-8)	1.447	-2.10(-8)
0.8600	1.436	-1.84(-7)	1.439	-1.86(-7)	1.442	-1.87(-7)	1.444	-1.89(-7)
1.0600	1.431	-1.55(-6)	1.433	-1.56(-6)	1.436	-1.57(-6)	1.439	-1.58(-6)
1.3000	1.421	-1.03(-5)	1.423	-1.04(-5)	1.426	-1.05(-5)	1.428	-1.05(-5)
1.5360	1.413	-1.41(-4)	1.416	-1.42(-4)	1.419	-1.43(-4)	1.421	-1.44(-4)
1.8000	1.400	-5.66(-4)	1.402	-5.70(-4)	1.405	-5.75(-4)	1.407	-5.79(-4)
2.0000	1.394	-0.00130	1.396	-0.00131	1.399	-0.00132	1.401	-0.00133
2.2500	1.379	-0.00185	1.382	-0.00187	1.384	-0.00188	1.386	-0.00189
2.5000	1.353	-0.00387	1.355	-0.00389	1.357	-0.00392	1.359	-0.00395
2.7000	1.310	-0.00586	1.312	-0.00589	1.314	-0.00594	1.316	-0.00597
3.0000	1.291	-0.0916	1.290	-0.0907	1.289	-0.0898	1.289	-0.0888
3.2000	1.302	-0.139	1.300	-0.140	1.298	-0.141	1.296	-0.142
3.3923	1.358	-0.168	1.360	-0.170	1.362	-0.172	1.363	-0.175
3.5000	1.379	-0.168	1.380	-0.170	1.381	-0.173	1.382	-0.175
3.7500	1.407	-0.146	1.410	-0.150	1.413	-0.154	1.416	-0.158
4.0000	1.416	-0.137	1.420	-0.140	1.424	-0.143	1.429	-0.146
4.5000	1.405	-0.136	1.410	-0.140	1.415	-0.144	1.420	-0.149
5.0000	1.384	-0.128	1.390	-0.130	1.396	-0.132	1.402	-0.134
5.5000	1.355	-0.189	1.360	-0.190	1.365	-0.191	1.369	-0.193
6.0000	1.453	-0.195	1.460	-0.195	1.467	-0.195	1.474	-0.195
6.2000	1.453	-0.156	1.460	-0.154	1.467	-0.152	1.474	-0.150
6.5000	1.394	-0.105	1.400	-0.100	1.406	-0.0952	1.412	-0.0906
7.2000	1.222	-0.171	1.225	-0.170	1.228	-0.169	1.231	-0.168
7.9000	1.144	-0.475	1.145	-0.472	1.146	-0.469	1.147	-0.466
8.2000	1.210	-0.674	1.212	-0.682	1.214	-0.690	1.217	-0.697
8.5000	1.411	-0.794	1.421	-0.804	1.431	-0.814	1.441	-0.824
8.7000	1.635	-0.793	1.661	-0.798	1.687	-0.803	1.713	-0.809
9.0000	1.705	-0.619	1.719	-0.616	1.733	-0.613	1.747	-0.609
9.2000	1.649	-0.572	1.661	-0.569	1.673	-0.566	1.685	-0.562
9.5000	1.727	-0.744	1.741	-0.742	1.755	-0.740	1.769	-0.739
9.8000	2.012	-0.569	2.038	-0.544	2.064	-0.520	2.089	-0.498
10.0000	1.986	-0.377	2.010	-0.360	2.034	-0.344	2.058	-0.328
10.5910	1.760	-0.271	1.770	-0.256	1.780	-0.242	1.790	-0.229
11.0000	1.742	-0.460	1.760	-0.454	1.778	-0.448	1.796	-0.442
11.5000	1.953	-0.278	1.969	-0.258	1.985	-0.240	2.001	-0.222
12.5000	1.772	-0.150	1.780	-0.140	1.788	-0.131	1.796	-0.122
13.0000	1.737	-0.150	1.749	-0.141	1.761	-0.132	1.773	-0.124
14.0000	1.686	-0.163	1.698	-0.156	1.710	-0.149	1.721	-0.143
14.8000	1.635	-0.184	1.641	-0.179	1.647	-0.174	1.653	-0.170
15.0000	1.621	-0.196	1.629	-0.193	1.637	-0.190	1.645	-0.186
16.4000	1.601	-0.436	1.621	-0.442	1.641	-0.448	1.661	-0.454
17.2000	1.855	-0.602	1.888	-0.605	1.921	-0.608	1.954	-0.611
18.0000	2.071	-0.268	2.101	-0.241	2.131	-0.217	2.161	-0.195
18.5000	1.981	-0.174	1.994	-0.152	2.007	-0.132	2.021	-0.115

Table A-1. (Cont.)

LAMBDA (μm)	260 K n_r	260 K n_i	250 K n_r	250 K n_i	240 K n_r	240 K n_i	230 K n_r	230 K n_i
20.0000	1.850	-0.118	1.860	-0.100	1.870	-0.0847	1.880	-0.0717
21.3000	1.799	-0.194	1.801	-0.182	1.803	-0.171	1.805	-0.160
22.5000	1.878	-0.236	1.892	-0.224	1.906	-0.213	1.921	-0.202
25.0000	1.912	-0.0865	1.930	-0.0670	1.948	-0.0519	1.966	-0.0402
27.9000	1.844	-0.0798	1.860	-0.0600	1.876	-0.0451	1.892	-0.0339
30.0000	1.794	-0.0930	1.810	-0.0700	1.826	-0.0527	1.842	-0.0396
35.0000	1.784	-0.139	1.800	-0.100	1.816	-0.0719	1.832	-0.0517
40.0000	2.012	-0.30	2.030	-0.250	2.048	-0.208	2.066	-0.173
50.0000	2.082	-0.405	2.100	-0.360	2.118	-0.320	2.136	-0.284
60.0000	2.082	-0.451	2.100	-0.400	2.118	-0.355	2.136	-0.314
80.0000	2.084	-0.459	2.100	-0.410	2.116	-0.366	2.132	-0.327
100.0000	2.092	-0.423	2.110	-0.380	2.128	-0.341	2.146	-0.307
150.0000	2.102	-0.322	2.120	-0.280	2.138	-0.244	2.156	-0.212
200.0000	2.104	-0.239	2.120	-0.200	2.136	-0.167	2.152	-0.140
300.0000	2.116	-0.131	2.130	-0.100	2.144	-0.0762	2.158	-0.0580

LAMBDA (μm)	220 K n_r	n_i	210 K n_r	n_i	200 K n_r	n_i	190 K n_r	n_i
0.2000	1.525	-1.07(-8)	1.528	-1.07(-8)	1.531	-1.08(-8)	1.535	-1.09(-8)
0.2500	1.510	-1.07(-8)	1.513	-1.07(-8)	1.516	-1.08(-8)	1.520	-1.09(-8)
0.3000	1.494	-1.06(-8)	1.497	-1.07(-8)	1.500	-1.08(-8)	1.503	-1.09(-8)
0.3371	1.483	-1.06(-8)	1.486	-1.07(-8)	1.489	-1.08(-8)	1.492	-1.09(-8)
0.4000	1.463	-1.06(-8)	1.466	-1.07(-8)	1.469	-1.08(-8)	1.472	-1.09(-8)
0.4880	1.455	-1.06(-8)	1.457	-1.07(-8)	1.460	-1.08(-8)	1.463	-1.09(-8)
0.5145	1.453	-1.06(-8)	1.456	-1.07(-8)	1.459	-1.08(-8)	1.462	-1.09(-8)
0.5500	1.452	-1.06(-8)	1.455	-1.07(-8)	1.458	-1.08(-8)	1.461	-1.09(-8)
0.6328	1.451	-1.56(-8)	1.454	-1.57(-8)	1.457	-1.58(-8)	1.460	-1.60(-8)
0.6943	1.450	-2.11(-8)	1.453	-2.13(-8)	1.456	-2.14(-8)	1.459	-2.16(-8)
0.8600	1.447	-1.90(-7)	1.450	-1.91(-7)	1.453	-1.93(-7)	1.455	-1.94(-7)
1.0600	1.442	-1.59(-6)	1.444	-1.60(-6)	1.447	-1.62(-6)	1.450	-1.63(-6)
1.3000	1.431	-1.06(-5)	1.434	-1.07(-5)	1.436	-1.08(-5)	1.439	-1.08(-5)
1.5360	1.424	-1.45(-4)	1.426	-1.46(-4)	1.429	-1.47(-4)	1.432	-1.48(-4)
1.8000	1.410	-5.83(-4)	1.412	-5.87(-4)	1.415	-5.91(-4)	1.417	-5.95(-4)
2.0000	1.404	-0.00134	1.406	-0.00134	1.409	-0.00135	1.411	-0.00136
2.2500	1.389	-0.00191	1.391	-0.00192	1.393	-0.00193	1.396	-0.00195
2.5000	1.361	-0.00398	1.363	-0.00400	1.366	-0.00403	1.368	-0.00406
2.7000	1.318	-0.00602	1.320	-0.00605	1.322	-0.00609	1.324	-0.00613
3.0000	1.288	-0.0879	1.288	-0.0870	1.287	-0.0861	1.286	-0.0853
3.2000	1.293	-0.143	1.291	-0.144	1.289	-0.145	1.287	-0.146
3.3923	1.365	-0.177	1.366	-0.179	1.368	-0.182	1.370	-0.184
3.5000	1.382	-0.178	1.383	-0.180	1.384	-0.183	1.385	-0.186
3.7500	1.418	-0.163	1.421	-0.167	1.424	-0.172	1.427	-0.176
4.0000	1.433	-0.149	1.438	-0.152	1.442	-0.156	1.446	-0.159
4.5000	1.425	-0.154	1.430	-0.158	1.435	-0.163	1.440	-0.168
5.0000	1.408	-0.136	1.414	-0.138	1.420	-0.140	1.426	-0.142
5.5000	1.374	-0.194	1.378	-0.196	1.383	-0.197	1.388	-0.199
6.0000	1.481	-0.195	1.488	-0.195	1.495	-0.195	1.502	-0.195
6.2000	1.482	-0.148	1.489	-0.146	1.496	-0.144	1.503	-0.142
6.5000	1.418	-0.0862	1.424	-0.0821	1.430	-0.0781	1.436	-0.0744
7.2000	1.234	-0.166	1.237	-0.165	1.240	-0.164	1.243	-0.163
7.9000	1.148	-0.463	1.149	-0.460	1.150	-0.457	1.151	-0.453
8.2000	1.219	-0.705	1.222	-0.713	1.224	-0.721	1.226	-0.729
8.5000	1.452	-0.835	1.462	-0.845	1.472	-0.856	1.482	-0.867
8.7000	1.740	-0.814	1.766	-0.819	1.792	-0.825	1.818	-0.830
9.0000	1.760	-0.606	1.774	-0.603	1.788	-0.599	1.802	-0.596
9.2000	1.698	-0.559	1.710	-0.556	1.722	-0.552	1.734	-0.549
9.5000	1.784	-0.737	1.798	-0.736	1.812	-0.734	1.826	-0.733
9.8000	2.115	-0.476	2.140	-0.455	2.166	-0.435	2.192	-0.416
10.0000	2.082	-0.313	2.106	-0.298	2.130	-0.285	2.154	-0.272
10.5910	1.800	-0.216	1.810	-0.204	1.820	-0.193	1.830	-0.182
11.0000	1.814	-0.436	1.832	-0.431	1.850	-0.425	1.868	-0.419
11.5000	2.016	-0.206	2.032	-0.192	2.048	-0.178	2.064	-0.165
12.5000	1.804	-0.114	1.812	-0.106	1.820	-0.0990	1.828	-0.0924
13.0000	1.784	-0.116	1.796	-0.109	1.808	-0.102	1.820	-0.0956
14.0000	1.733	-0.137	1.744	-0.131	1.756	-0.125	1.768	-0.120
14.8000	1.660	-0.165	1.666	-0.161	1.672	-0.156	1.678	-0.152
15.0000	1.652	-0.183	1.660	-0.180	1.668	-0.177	1.676	-0.173
16.4000	1.682	-0.460	1.702	-0.466	1.722	-0.472	1.742	-0.478
17.2000	1.986	-0.614	2.019	-0.617	2.052	-0.620	2.085	-0.624
18.0000	2.192	-0.175	2.222	-0.158	2.252	-0.142	2.282	-0.127
18.5000	2.034	-0.101	2.048	-0.0878	2.061	-0.0765	2.074	-0.0667

Table A-1. (Cont.)

LAMBDA	220 K		210 K		200 K		190 K	
(μm)	n_r	n_i	n_r	n_i	n_r	n_i	n_r	n_i
20.0000	1.890	-0.0607	1.900	-0.0514	1.910	-0.0435	1.920	-0.0368
21.3000	1.808	-0.150	1.810	-0.141	1.812	-0.132	1.814	-0.124
22.5000	1.935	-0.192	1.950	-0.182	1.964	-0.173	1.978	-0.164
25.0000	1.984	-0.0312	2.002	-0.0241	2.020	-0.0187	2.038	-0.0145
27.9000	1.908	-0.0255	1.924	-0.0192	1.940	-0.0144	1.956	-0.0108
30.0000	1.858	-0.0298	1.874	-0.0225	1.890	-0.0169	1.906	-0.0127
35.0000	1.848	-0.0372	1.864	-0.0267	1.880	-0.0192	1.896	-0.0138
40.0000	2.084	-0.144	2.102	-0.119	2.120	-0.0992	2.138	-0.0825
50.0000	2.154	-0.253	2.172	-0.224	2.190	-0.199	2.208	-0.177
60.0000	2.154	-0.279	2.172	-0.247	2.190	-0.219	2.208	-0.194
80.0000	2.148	-0.292	2.164	-0.261	2.180	-0.233	2.196	-0.209
100.0000	2.164	-0.275	2.182	-0.247	2.200	-0.222	2.218	-0.200
150.0000	2.174	-0.185	2.192	-0.161	2.210	-0.140	2.228	-0.122
200.0000	2.168	-0.117	2.184	-0.0977	2.200	-0.0816	2.216	-0.0682
300.0000	2.172	-0.0442	2.186	-0.0337	2.200	-0.0256	2.214	-0.0195

Table A-1. (Cont.)

LAMBDA	180 K		170 K		160 K		150 K	
(μm)	n_r	n_i	n_r	n_i	n_r	n_i	n_r	n_i
0.2000	1.538	-1.10(-8)	1.542	-1.11(-8)	1.545	-1.12(-8)	1.549	-1.13(-8)
0.2500	1.523	-1.10(-8)	1.526	-1.11(-8)	1.529	-1.12(-8)	1.533	-1.12(-8)
0.3000	1.506	-1.10(-8)	1.510	-1.11(-8)	1.513	-1.11(-8)	1.516	-1.12(-8)
0.3371	1.495	-1.10(-8)	1.499	-1.10(-8)	1.502	-1.11(-8)	1.505	-1.12(-8)
0.4000	1.475	-1.09(-8)	1.478	-1.10(-8)	1.480	-1.11(-8)	1.483	-1.12(-8)
0.4880	1.466	-1.09(-8)	1.469	-1.10(-8)	1.472	-1.11(-8)	1.474	-1.12(-8)
0.5145	1.465	-1.09(-8)	1.468	-1.10(-8)	1.470	-1.11(-8)	1.473	-1.12(-8)
0.5500	1.464	-1.09(-8)	1.467	-1.10(-8)	1.469	-1.11(-8)	1.472	-1.12(-8)
0.6328	1.463	-1.61(-8)	1.465	-1.62(-8)	1.468	-1.63(-8)	1.471	-1.64(-8)
0.6943	1.461	-2.18(-8)	1.464	-2.19(-8)	1.467	-2.21(-8)	1.470	-2.22(-8)
0.8600	1.458	-1.96(-7)	1.461	-1.97(-7)	1.464	-1.99(-7)	1.467	-2.00(-7)
1.0600	1.453	-1.64(-6)	1.455	-1.65(-6)	1.458	-1.66(-6)	1.461	-1.68(-6)
1.3000	1.442	-1.09(-5)	1.444	-1.10(-5)	1.447	-1.11(-5)	1.450	-1.12(-5)
1.5360	1.434	-1.50(-4)	1.437	-1.51(-4)	1.439	-1.52(-4)	1.442	-1.53(-4)
1.8000	1.420	-6.00(-4)	1.423	-6.04(-4)	1.425	-6.08(-4)	1.428	-6.12(-4)
2.0000	1.413	-0.00137	1.416	-0.00138	1.418	-0.00139	1.421	-0.00140
2.2500	1.398	-0.00196	1.401	-0.00197	1.403	-0.00199	1.405	-0.00200
2.5000	1.370	-0.00408	1.372	-0.00411	1.374	-0.00414	1.376	-0.00417
2.7000	1.325	-0.00617	1.327	-0.00621	1.329	-0.00625	1.331	-0.00630
3.0000	1.286	-0.0844	1.285	-0.0835	1.285	-0.0827	1.284	-0.0818
3.2000	1.285	-0.147	1.282	-0.148	1.280	-0.149	1.278	-0.151
3.3923	1.371	-0.187	1.373	-0.189	1.374	-0.192	1.376	-0.194
3.5000	1.386	-0.188	1.386	-0.191	1.387	-0.194	1.388	-0.197
3.7500	1.430	-0.181	1.432	-0.186	1.435	-0.191	1.438	-0.197
4.0000	1.451	-0.162	1.455	-0.166	1.460	-0.169	1.464	-0.173
4.5000	1.445	-0.174	1.450	-0.179	1.455	-0.185	1.460	-0.191
5.0000	1.432	-0.144	1.438	-0.146	1.444	-0.148	1.450	-0.150
5.5000	1.392	-0.200	1.397	-0.202	1.401	-0.203	1.406	-0.205
6.0000	1.509	-0.195	1.516	-0.195	1.523	-0.195	1.530	-0.195
6.2000	1.510	-0.140	1.518	-0.138	1.525	-0.136	1.532	-0.134
6.5000	1.442	-0.0708	1.448	-0.0674	1.454	-0.0641	1.460	-0.0610
7.2000	1.246	-0.162	1.249	-0.161	1.252	-0.160	1.255	-0.159
7.9000	1.152	-0.450	1.153	-0.447	1.154	-0.445	1.155	-0.442
8.2000	1.229	-0.737	1.231	-0.746	1.234	-0.754	1.236	-0.762
8.5000	1.492	-0.878	1.503	-0.889	1.513	-0.900	1.523	-0.912
8.7000	1.844	-0.836	1.871	-0.841	1.897	-0.847	1.923	-0.853
9.0000	1.816	-0.593	1.829	-0.590	1.843	-0.587	1.857	-0.583
9.2000	1.746	-0.546	1.759	-0.543	1.771	-0.540	1.783	-0.536
9.5000	1.840	-0.731	1.855	-0.729	1.869	-0.728	1.883	-0.726
9.8000	2.217	-0.398	2.243	-0.381	2.268	-0.364	2.294	-0.348
10.0000	2.178	-0.259	2.202	-0.247	2.226	-0.236	2.250	-0.225
10.5910	1.840	-0.172	1.850	-0.163	1.860	-0.154	1.870	-0.145
11.0000	1.886	-0.414	1.904	-0.408	1.922	-0.403	1.940	-0.398
11.5000	2.080	-0.153	2.095	-0.142	2.111	-0.132	2.127	-0.123
12.5000	1.836	-0.0862	1.844	-0.0804	1.852	-0.0750	1.860	-0.0700
13.0000	1.832	-0.0896	1.843	-0.0839	1.855	-0.0787	1.867	-0.0737
14.0000	1.779	-0.114	1.791	-0.109	1.802	-0.105	1.814	-0.100
14.8000	1.684	-0.148	1.691	-0.144	1.697	-0.140	1.703	-0.136
15.0000	1.684	-0.170	1.691	-0.167	1.699	-0.164	1.707	-0.161
16.4000	1.762	-0.484	1.783	-0.491	1.803	-0.497	1.823	-0.504
17.2000	2.118	-0.627	2.150	-0.630	2.183	-0.633	2.216	-0.636
18.0000	2.312	-0.115	2.343	-0.103	2.373	-0.0926	2.403	-0.0833
18.5000	2.088	-0.0581	2.101	-0.0507	2.115	-0.0442	2.128	-0.0385

Table A-1. (Cont.)

LAMBDA (μm)	180 K		170 K		160 K		150 K	
	n_r	n_i	n_r	n_i	n_r	n_i	n_r	n_i
20.0000	1.930	-0.312	1.940	-0.0264	1.950	-0.0223	1.960	-0.0189
21.3000	1.816	-0.117	1.819	-0.110	1.821	-0.103	1.823	-0.0965
22.5000	1.993	-0.156	2.007	-0.148	2.022	-0.141	2.036	-0.134
25.0000	2.056	-0.0112	2.074	-0.00870	2.092	-0.00674	2.110	-0.00522
27.9000	1.972	-0.00814	1.988	-0.00612	2.004	-0.00460	2.020	-0.00346
30.0000	1.922	-0.00957	1.938	-0.00720	1.954	-0.00542	1.970	-0.00408
35.0000	1.912	-0.00994	1.928	-0.00715	1.944	-0.00514	1.960	-0.00370
40.0000	2.156	-0.0685	2.174	-0.0570	2.192	-0.0474	2.210	-0.0394
50.0000	2.226	-0.157	2.244	-0.140	2.262	-0.124	2.280	-0.110
60.0000	2.226	-0.172	2.244	-0.153	2.262	-0.135	2.280	-0.120
80.0000	2.212	-0.186	2.228	-0.167	2.244	-0.149	2.260	-0.133
100.0000	2.236	-0.179	2.254	-0.161	2.272	-0.145	2.290	-0.130
150.0000	2.246	-0.106	2.264	-0.0924	2.282	-0.0804	2.300	-0.0700
200.0000	2.232	-0.0570	2.248	-0.0477	2.264	-0.0399	2.280	-0.0333
300.0000	2.228	-0.0149	2.242	-0.0113	2.256	-0.00863	2.270	-0.00657

Table A-2. Radiative Parameters for the Proposed Background
Stratospheric Aerosol Model at 180 K

LAMBDA (μm)	INDEX OF REFRACTION n_r	n_i	EXTINCTION (km^{-1})	SCATTERING (km^{-1})	ABSORPTION (km^{-1})	SINGLE SCATTERING ALBEDO	ASYMMETRY PARAMETER
0.2000	1.5380	0.0000	7.9699(-4)	7.9699(-4)	9.6982(-11)	1.0000	0.6675
0.2500	1.5230	0.0000	7.7672(-4)	7.7672(-4)	7.5243(-11)	1.0000	0.6781
0.3000	1.5060	0.0000	7.2236(-4)	7.2236(-4)	5.9702(-11)	1.0000	0.6880
0.3371	1.4950	0.0000	6.7058(-4)	6.7058(-4)	5.1780(-11)	1.0000	0.6926
0.4000	1.4750	0.0000	5.7243(-4)	5.7243(-4)	4.1127(-11)	1.0000	0.6976
0.4880	1.4660	0.0000	4.5886(-4)	4.5886(-4)	3.1715(-11)	1.0000	0.6894
0.5145	1.4650	0.0000	4.2960(-4)	4.2960(-4)	2.9518(-11)	1.0000	0.6857
0.5500	1.4640	0.0000	3.9352(-4)	3.9352(-4)	2.7100(-11)	1.0000	0.6799
0.6328	1.4630	0.0000	3.2188(-4)	3.2188(-4)	3.3437(-11)	1.0000	0.6648
0.6943	1.4610	0.0000	2.7659(-4)	2.7659(-4)	3.9996(-11)	1.0000	0.6537
0.8600	1.4580	0.0000	1.8749(-4)	1.8749(-4)	2.6829(-10)	1.0000	0.6220
1.0600	1.4530	0.0000	1.2017(-4)	1.2017(-4)	1.6755(-9)	1.0000	0.5838
1.3000	1.4420	0.0000	7.1902(-5)	7.1892(-5)	8.3428(-9)	1.0000	0.5391
1.5360	1.4340	-0.0002	4.5632(-5)	4.5540(-5)	9.1062(-8)	0.9980	0.4960
1.8000	1.4200	-0.0006	2.8028(-5)	2.7734(-5)	2.9353(-7)	0.9900	0.4500
2.0000	1.4130	-0.0014	2.0394(-5)	1.9811(-5)	5.8329(-7)	0.9710	0.4168
2.2500	1.3980	-0.0020	1.3666(-5)	1.2948(-5)	7.1821(-7)	0.9470	0.3778
2.5000	1.3700	-0.0041	9.3672(-6)	8.0509(-6)	1.3163(-6)	0.8590	0.3394
2.7000	1.3250	-0.0062	6.6808(-6)	4.8493(-6)	1.8315(-6)	0.7260	0.3076
3.0000	1.2860	-0.0844	2.4662(-5)	2.6705(-6)	2.1991(-5)	0.1080	0.2600
3.2000	1.2850	-0.1470	3.7709(-5)	2.3908(-6)	3.5317(-5)	0.0630	0.2341
3.3923	1.3710	-0.1870	4.3865(-5)	3.2291(-6)	4.0637(-5)	0.0740	0.2231
3.5000	1.3860	-0.1880	4.2365(-5)	3.1162(-6)	3.9249(-5)	0.0740	0.2160
3.7500	1.4300	-0.1810	3.7340(-5)	2.9396(-6)	3.4401(-5)	0.0790	0.2025
4.0000	1.4510	-0.1620	3.0971(-5)	2.5219(-6)	2.8448(-5)	0.0810	0.1888
4.5000	1.4450	-0.1740	2.8559(-5)	1.6692(-6)	2.6891(-5)	0.0580	0.1565
5.0000	1.4320	-0.1440	2.1086(-5)	1.0612(-6)	2.0024(-5)	0.0500	0.1307
5.5000	1.3920	-0.2000	2.6317(-5)	6.9919(-7)	2.5617(-5)	0.0270	0.1066
6.0000	1.5090	-0.1950	2.1943(-5)	7.5469(-7)	2.1187(-5)	0.0340	0.0976
6.2000	1.5100	-0.1400	1.5341(-5)	6.3498(-7)	1.4705(-5)	0.0410	0.0923
6.5000	1.4420	-0.0708	7.7921(-6)	3.9397(-7)	7.3983(-6)	0.0510	0.0812
7.2000	1.2460	-0.1620	1.7148(-5)	1.2083(-7)	1.7027(-5)	0.0070	0.0598
7.9000	1.1520	-0.4500	4.6008(-5)	2.3177(-7)	4.5776(-5)	0.0050	0.0460
8.2000	1.2290	-0.7370	7.0052(-5)	5.4643(-7)	6.9506(-5)	0.0080	0.0411
8.5000	1.4920	-0.8780	6.4218(-5)	7.0379(-7)	6.3515(-5)	0.0110	0.0420
8.7000	1.8440	-0.8360	4.4974(-5)	7.1556(-7)	4.4257(-5)	0.0160	0.0503
9.0000	1.8160	-0.5930	3.2714(-5)	4.6127(-7)	3.2252(-5)	0.0140	0.0499
9.2000	1.7460	-0.5460	3.1225(-5)	3.6989(-7)	3.0857(-5)	0.0120	0.0463
9.5000	1.8400	-0.7310	3.6487(-5)	4.4686(-7)	3.6041(-5)	0.0120	0.0438
9.8000	2.2170	-0.3980	1.5095(-5)	4.2208(-7)	1.4673(-5)	0.0280	0.0562
10.0000	2.1780	-0.2590	1.0092(-5)	3.5474(-7)	9.7377(-6)	0.0350	0.0534
10.59.0	1.8400	-0.1720	8.1515(-6)	1.7248(-7)	7.9789(-6)	0.0210	0.0388
11.00C0	1.8860	-0.4140	1.7710(-5)	1.8681(-7)	1.7523(-5)	0.0110	0.0360
11.5000	2.0800	-0.1530	5.5475(-6)	1.7380(-7)	5.3738(-6)	0.0310	0.0378
12.5000	1.8360	-0.0862	3.4629(-6)	8.5025(-8)	3.3778(-6)	0.0250	0.0278
13.0000	1.8320	-0.0896	3.4530(-6)	7.2077(-8)	3.3810(-6)	0.0210	0.0256
14.0000	1.7790	-0.1140	4.2023(-6)	4.8790(-8)	4.1535(-6)	0.0120	0.0214
14.8000	1.6840	-0.1480	5.5184(-6)	3.2617(-8)	5.4858(-6)	0.0060	0.0182
15.0000	1.6840	-0.1700	6.2432(-6)	3.1351(-8)	6.2118(-6)	0.0050	0.0177
16.4000	1.7620	-0.4840	1.4921(-5)	3.4490(-8)	1.4887(-5)	0.0020	0.0149
17.2000	2.1180	-0.6270	1.3428(-5)	4.5155(-8)	1.3383(-5)	0.0030	0.0161
18.0000	2.3120	-0.1150	2.1296(-6)	3.5360(-8)	2.0942(-6)	0.0170	0.0172
18.5000	2.0880	-0.0581	1.2619(-6)	2.4983(-8)	1.2369(-6)	0.0200	0.0145
20.0000	1.9300	-0.3120	6.9302(-6)	1.6357(-8)	6.9140(-6)	0.0020	0.0112
21.3000	1.8160	-0.1170	2.7031(-6)	9.6397(-9)	2.6935(-6)	0.0040	0.0094

Table A-2.   (Continued)

LAMBDA (μm)	INDEX OF REFRACTION n_r	n_i	EXTINCTION (km^{-1})	SCATTERING (km^{-1})	ABSORPTION (km^{-1})	SINGLE SCATTERING ALBEDO	ASYMMETRY PARAMETER
22.5000	1.9930	-0.1560	2.9443(-6)	1.0256(-8)	2.9340(-6)	0.0030	0.0092
25.0000	2.0560	-0.0112	1.8728(-7)	7.1129(-9)	1.8017(-7)	0.0380	0.0078
27.9000	1.9720	-0.0081	1.2970(-7)	4.0942(-9)	1.2561(-7)	0.0320	0.0060
30.0000	1.9220	-0.0096	1.4588(-7)	2.8441(-9)	1.4303(-7)	0.0190	0.0050
35.0000	1.9120	-0.0099	1.2976(-7)	1.5090(-9)	1.2825(-7)	0.0120	0.0037
40.0000	2.1560	-0.0685	6.3187(-7)	1.2124(-9)	6.3066(-7)	0.0020	0.0032
50.0000	2.2260	-0.1570	1.0877(-6)	5.3886(-10)	1.0872(-6)	0.0000	0.0021
60.0000	2.2260	-0.1720	9.9159(-7)	2.6038(-10)	9.9132(-7)	0.0000	0.0015
80.0000	2.2120	-0.1860	8.1250(-7)	8.1470(-11)	8.1242(-7)	0.0000	0.0008
100.0000	2.2360	-0.1790	6.1317(-7)	3.4056(-11)	6.1314(-7)	0.0000	0.0005
150.0000	2.2460	-0.1060	2.4061(-7)	6.7002(-12)	2.4059(-7)	0.0000	0.0002
200.0000	2.2320	-0.0570	9.8257(-8)	2.0813(-12)	9.8255(-8)	0.0000	0.0001
300.0000	2.2280	-0.0149	1.7185(-8)	4.0871(-13)	1.7185(-8)	0.0000	0.0001

Table A-3. Radiative Parameters for the Proposed Background Stratospheric Aerosol Model at 250 K

LAMBDA (μm)	INDEX OF REFRACTION n_r	n_i	EXTINCTION (km^{-1})	SCATTERING (km^{-1})	ABSORPTION (km^{-1})	SINGLE SCATTERING ALBEDO	ASYMMETRY PARAMETER
0.2000	1.5150	0.0000	8.4896(-4)	8.4896(-4)	9.7798(-11)	1.0000	0.6811
0.2500	1.5000	0.0000	8.1890(-4)	8.1890(-4)	7.3554(-11)	1.0000	0.6927
0.3000	1.4840	0.0000	7.5494(-4)	7.5494(-4)	5.9212(-11)	1.0000	0.7014
0.3371	1.4740	0.0000	6.9694(-4)	6.9694(-4)	5.1558(-11)	1.0000	0.7050
0.4000	1.4540	0.0000	5.8792(-4)	5.8792(-4)	4.0576(-11)	1.0000	0.7093
0.4880	1.4460	0.0000	4.6722(-4)	4.6722(-4)	3.1562(-11)	1.0000	0.6995
0.5145	1.4450	0.0000	4.3658(-4)	4.3658(-4)	2.9544(-11)	1.0000	0.6952
0.5500	1.4440	0.0000	3.9860(-4)	3.9860(-4)	2.7082(-11)	1.0000	0.6892
0.6328	1.4430	0.0000	3.2406(-4)	3.2406(-4)	3.3268(-11)	1.0000	0.6732
0.6943	1.4420	0.0000	2.7826(-4)	2.7826(-4)	3.9798(-11)	1.0000	0.6611
0.8600	1.4390	0.0000	1.8726(-4)	1.8726(-4)	2.6786(-10)	1.0000	0.6279
1.0600	1.4330	0.0000	1.1879(-4)	1.1879(-4)	1.6825(-9)	1.0000	0.5883
1.3000	1.4230	0.0000	7.0870(-5)	7.0862(-5)	8.4408(-9)	1.0000	0.5417
1.5360	1.4160	-0.0001	4.4988(-5)	4.4896(-5)	9.1746(-8)	0.9980	0.4971
1.8000	1.4020	-0.0006	2.7508(-5)	2.7212(-5)	2.9766(-7)	0.9890	0.4498
2.0000	1.3960	-0.0013	2.0086(-5)	1.9491(-5)	5.9648(-7)	0.9700	0.4160
2.2500	1.3820	-0.0019	1.3491(-5)	1.2757(-5)	7.3408(-7)	0.9460	0.3765
2.5000	1.3550	-0.0039	9.2710(-6)	7.9252(-6)	1.3460(-6)	0.8550	0.3377
2.7000	1.3120	-0.0059	6.6542(-6)	4.7786(-6)	1.8756(-6)	0.7180	0.3060
3.0000	1.2900	-0.0907	2.8158(-5)	2.9478(-6)	2.5210(-5)	0.1050	0.2598
3.2000	1.3000	-0.1400	3.8576(-5)	2.7390(-6)	3.5838(-5)	0.0710	0.2365
3.3923	1.3600	-0.1700	4.3002(-5)	3.2116(-6)	3.9790(-5)	0.0750	0.2235
3.5000	1.3800	-0.1700	4.1328(-5)	3.1722(-6)	3.8156(-5)	0.0770	0.2170
3.7500	1.4100	-0.1500	3.3712(-5)	2.8130(-6)	3.0900(-5)	0.0830	0.2028
4.0000	1.4200	-0.1400	2.9106(-5)	2.3418(-6)	2.6766(-5)	0.0800	0.1868
4.5000	1.4100	-0.1400	2.5138(-5)	1.4994(-6)	2.3638(-5)	0.0600	0.1544
5.0000	1.3900	-0.1300	2.0744(-5)	9.3814(-7)	1.9806(-5)	0.0450	0.1276
5.5000	1.3600	-0.1900	2.7162(-5)	6.4632(-7)	2.6516(-5)	0.0240	0.1048
6.0000	1.4600	-0.1950	2.4064(-5)	6.8874(-7)	2.3376(-5)	0.0290	0.0947
6.2000	1.4600	-0.1540	1.8431(-5)	5.7902(-7)	1.7852(-5)	0.0310	0.0894
6.5000	1.4000	-0.1000	1.1819(-5)	3.6004(-7)	1.1459(-5)	0.0300	0.0792
7.2000	1.2250	-0.1700	1.9441(-5)	1.1903(-7)	1.9322(-5)	0.0060	0.0592
7.9000	1.1450	-0.4720	5.1906(-5)	2.6960(-7)	5.1636(-5)	0.0050	0.0456
8.2000	1.2120	-0.6820	7.0128(-5)	4.9898(-7)	6.9630(-5)	0.0070	0.0415
8.5000	1.4210	-0.8040	6.7380(-5)	6.3630(-7)	6.6744(-5)	0.0090	0.0415
8.7000	1.6610	-0.7980	5.3624(-5)	6.5252(-7)	5.2972(-5)	0.0120	0.0457
9.0000	1.7190	-0.6160	3.9094(-5)	4.5970(-7)	3.8634(-5)	0.0120	0.0468
9.2000	1.6610	-0.5690	3.7092(-5)	3.6976(-7)	3.6722(-5)	0.0100	0.0438
9.5000	1.7410	-0.7420	4.2838(-5)	4.5084(-7)	4.2386(-5)	0.0110	0.0412
9.8000	2.0380	-0.5440	2.4720(-5)	4.1680(-7)	2.4304(-5)	0.0170	0.0488
10.0000	2.0100	-0.3600	1.6740(-5)	3.2878(-7)	1.6411(-5)	0.0200	0.0475
10.5910	1.7700	-0.2560	1.3545(-5)	1.7156(-7)	1.3373(-5)	0.0130	0.0370
11.0000	1.7600	-0.4540	2.2850(-5)	1.7655(-7)	2.2674(-5)	0.0080	0.0333
11.5000	1.9690	-0.2580	1.0709(-5)	1.6735(-7)	1.0542(-5)	0.0160	0.0352
12.5000	1.7800	-0.1400	6.2102(-6)	8.3484(-8)	6.1266(-6)	0.0130	0.0269
13.0000	1.7490	-0.1410	6.1382(-6)	6.7122(-8)	6.0710(-6)	0.0110	0.0244
14.0000	1.6980	-0.1560	6.5200(-6)	4.5188(-8)	6.4748(-6)	0.0070	0.0205
14.8000	1.6410	-0 1790	7.3654(-6)	3.2374(-8)	7.3330(-6)	0.0040	0.0177
15.0000	1.6290	-0.1930	7.8992(-6)	3.0202(-8)	7.8690(-6)	0.0040	0.0172
16.4000	1.6210	-0.4420	1.6408(-5)	2.8794(-8)	1.6379(-5)	0.0020	0.0139
17.2000	1.8880	-0.6050	1.6851(-5)	·3.9700(-8)	1.6811(-5)	0.0020	0.0142
18.0000	2.1010	-0.2410	5.5800(-6)	3.1632(-8)	5.5482(-6)	0.0060	0.0153
18.5000	1.9940	-0.1520	3.7548(-6)	2.4154(-8)	3.7308(-6)	0.0060	0.0137
20.0000	1.8600	-0.1000	2.5476(-6)	1.4246(-8)	2.5334(-6)	0.0060	0.0109
21.3000	1.8010	-0.1820	4.5384(-6)	1.0341(-8)	4.5280(-6)	0.0020	0.0093

Table A-3. (Continued)

LAMBDA (μm)	INDEX OF REFRACTION n_r	n_i	EXTINCTION (km^{-1})	SCATTERING (km^{-1})	ABSORPTION (km^{-1})	SINGLE SCATTERING ALBEDO	ASYMMETRY PARAMETER
22.5000	1.8920	-0.2240	4.8942(-6)	9.8082(-9)	4.8844(-6)	0.0020	0.0087
25.0000	1.9300	-0.0670	1.2850(-6)	6.4360(-9)	1.2786(-6)	0.0050	0.0073
27.9000	1.8600	-0.0600	1.0893(-6)	3.7050(-9)	1.0856(-6)	0.0030	0.0056
30.0000	1.8100	-0.0700	1.2287(-6)	2.5440(-9)	1.2261(-6)	0.0020	0.0047
35.0000	1.8000	-0.1000	1.5128(-6)	1.3574(-9)	1.5115(-6)	0.0010	0.0035
40.0000	2.0300	-0.2500	2.7168(-6)	1.1800(-9)	2.7156(-6)	0.0000	0.0030
50.0000	2.1000	-0.3600	2.9246(-6)	5.4842(-10)	2.9240(-6)	0.0000	0.0019
60.0000	2.1000	-0.4000	2.6962(-6)	2.7004(-10)	2.6958(-6)	0.0000	0.0013
80.0000	2.1000	-0.4100	2.0692(-6)	8.5846(-11)	2.0692(-6)	0.0000	0.0008
100.0000	2.1100	-0.3800	1.5255(-6)	3.4882(-11)	1.5254(-6)	0.0000	0.0005
150.0000	2.1200	-0.2800	7.4886(-7)	6.6320(-12)	7.4886(-7)	0.0000	0.0002
200.0000	2.1200	-0.2000	4.0300(-7)	2.0390(-12)	4.0300(-7)	0.0000	0.0001
300.0000	2.1300	-0.1000	1.3368(-7)	3.9794(-13)	1.3368(-7)	0.0000	0.0001